AGU PUBLICATIONS

Geochemistry, Geophysics, Geosystems

RESEARCH ARTICLE
10.1002/2014GC005402

Key Points:
- Biostratigraphy, isotope geochemistry, and clast componentry of IODP Site U1396
- Deposits are correlated across sites to the south and south west of Montserrat
- Results highlight the spatial heterogeneity of deposits around volcanic islands

Correspondence to:
D. Wall-Palmer,
deborah.wall-palmer@plymouth.ac.uk

Citation:
Wall-Palmer, D., et al. (2014), Late Pleistocene stratigraphy of IODP Site U1396 and compiled chronology offshore of south and south west Montserrat, Lesser Antilles, *Geochem. Geophys. Geosyst.*, *15*, 3000–3020, doi:10.1002/2014GC005402.

Received 5 MAY 2014
Accepted 2 JUL 2014
Accepted article online 8 JUL 2014
Published online 25 JUL 2014

Late Pleistocene stratigraphy of IODP Site U1396 and compiled chronology offshore of south and south west Montserrat, Lesser Antilles

Deborah Wall-Palmer[1], Maya Coussens[2], Peter J. Talling[2], Martin Jutzeler[2], Michael Cassidy[3], Isabelle Marchant[3], Martin R. Palmer[3], Sebastian F. L. Watt[4], Christopher W. Smart[1], Jodie K. Fisher[1], Malcolm B. Hart[1], Andrew Fraass[5], Jessica Trofimovs[6], Anne Le Friant[7], Osamu Ishizuka[8], Tatsuya Adachi[9], Mohammed Aljahdali[10], Georges Boudon[11], Christoph Breitkreuz[12], Daisuke Endo[13], Akihiko Fujinawa[14], Robert Hatfield[15], Matthew J. Hornbach[16], Kyoko Kataoka[17], Sara Lafuerza[18], Fukashi Maeno[19], Michael Manga[20], Michael Martinez-Colon[21], Molly McCanta[22], Sally Morgan[23], Takeshi Saito[24], Angela L. Slagle[25], Adam J. Stinton[26,27], K. S. V. Subramanyam[28], Yoshihiko Tamura[29], Benoit Villemant[30], and Fei Wang[31]

[1]School of Geography, Earth, and Environmental Sciences, Plymouth University, Plymouth, UK, [2]National Oceanography Centre, Southampton, UK, [3]School of Ocean and Earth Science, University of Southampton, Southampton, UK, [4]School of Geography, Earth, and Environmental Sciences, University of Birmingham, Birmingham, UK, [5]Department of Geosciences, University of Massachusetts-Amherst, Amherst, Massachusetts, USA, [6]Science and Engineering Faculty, Queensland University of Technology, Brisbane, Queensland, Australia, [7]Institut de Physique du Globe de Paris, Sorbonne Paris Cité and CNRS UMR 7154, Paris, France, [8]Geological Survey of Japan (AIST), Ibaraki, Japan, [9]Japan Conservation Engineers, Co. Ltd., Hokkaido, Japan, [10]Department of Earth, Ocean, and Atmospheric Sciences, Florida State University, Tallahassee, Florida, USA, [11]Équipe de Géologie des Systèmes Volcaniques, Institut de Physique du Globe de Paris, Sorbonne Paris Cité, UMR 7154 CNRS, Paris, France, [12]Physical Volcanology and Sedimentology, Institut für Geologie und Paläontologie, Technische Universität Bergakademie Freiberg, Freiberg, Germany, [13]A203, Earth Evolution Sciences, University of Tsukuba, Ibaraki, Japan, [14]Department of Earth Sciences, Ibaraki University, Ibaraki, Japan, [15]CEOAS, Oregon State University, Corvallis, Oregon, USA, [16]Institute for Geophysics, University of Texas at Austin, Austin, Texas, USA, [17]Research Institute for Natural Hazards and Disaster Recovery, Niigata University, Niigata, Japan, [18]Institut de Physique du Globe de Paris, Sorbonne Paris Cité, Universite Paris Diderot, UMR 7175, CNRS, Paris, France, [19]Volcano Research Center, Earthquake Research Institute, University of Tokyo, Tokyo, Japan, [20]Department of Earth and Planetary Science, University of California, Berkeley, Berkeley, California, USA, [21]College of Marine Science, University of South Florida, St. Petersburg, Florida, USA, [22]Department of Geology, Tufts University, Medford, Massachusetts, USA, [23]Department of Geology, University of Leicester, Leicester, UK, [24]Department of Geology, Faculty of Science, Shinshu University, Matsumoto, Japan, [25]Borehole Research Group, Lamont-Doherty Earth Observatory of Columbia University, Palisades, New York, USA, [26]Montserrat Volcano Observatory, Flemmings, Montserrat, West Indies, [27]Seismic Research Center, University of the West Indies, St. Augustine, Trinidad and Tobago, [28]Geochemistry Division, National Geophysical Research Institute, Hyderabad, Andhra Pradesh, India, [29]Institute for Research on Earth Evolution, JAMSTEC, Yokosuka, Japan, [30]Laboratoire de Petrologie, Geochimie, Volcanologie, University Pierre et Marie Curie–Paris 6, UMR 7193, ISTEP, Paris, France, [31]Institute of Geology and Geophysics, Chinese Academy of Sciences, Beijing, China

Abstract Marine sediments around volcanic islands contain an archive of volcaniclastic deposits, which can be used to reconstruct the volcanic history of an area. Such records hold many advantages over often incomplete terrestrial data sets. This includes the potential for precise and continuous dating of intervening sediment packages, which allow a correlatable and temporally constrained stratigraphic framework to be constructed across multiple marine sediment cores. Here we discuss a marine record of eruptive and mass-wasting events spanning ~250 ka offshore of Montserrat, using new data from IODP Expedition 340, as well as previously collected cores. By using a combination of high-resolution oxygen isotope stratigraphy, AMS radiocarbon dating, biostratigraphy of foraminifera and calcareous nannofossils, and clast componentry, we identify five major events at Soufriere Hills volcano since 250 ka. Lateral correlations of these events across sediment cores collected offshore of the south and south west of Montserrat have improved our understanding of the timing, extent and associations between events in this area. Correlations reveal that powerful and potentially erosive density-currents traveled at least 33 km offshore and demonstrate that marine deposits, produced by eruption-fed and mass-wasting events on volcanic islands, are heterogeneous in their spatial distribution. Thus, multiple drilling/coring sites are needed to reconstruct the full chronostratigraphy of volcanic islands. This multidisciplinary study will be vital to interpreting the chaotic records of

submarine landslides at other sites drilled during Expedition 340 and provides a framework that can be applied to the stratigraphic analysis of sediments surrounding other volcanic islands.

1. Introduction

Volcanic islands can be the source of hazardous eruptions and undergo flank collapses that generate offshore debris avalanche deposits and associated tsunamis [*Masson et al*., 2006]. Deposits derived from a variety of mass-wasting processes, including large landslides, have been identified from a number of volcanic islands, including the Aleutian Islands [*Waythomas et al*., 2009], Hawaii [*Moore et al*., 1994], Ritter Island, Papua New Guinea [*Silver et al*., 2005], the Canary Islands [*Hunt et al*., 2011], and Ischia [*Chiocci and De Alteriis*, 2006], demonstrating that the interaction of volcanic processes with the marine environment is widespread. It is, therefore, important to understand the chronology of past events at a volcanic island to assess the most likely future hazards, their frequency, and temporal variation in activity. The subaerial record of volcanic activity and collapses can be difficult to decode, due to burial or erosion by later events. Indeed, most of the erupted material at volcanic islands may end up in the ocean [*Le Friant et al*., 2008, 2010]. Volcanic eruptions may deposit volcanic clasts at tens of kilometers offshore by means of density-currents that cross the shore transition [*Trofimovs et al*., 2006; *Allen et al*., 2012; *Schindlbeck et al*., 2013] and/or tephra fallout onto water [*Alloway et al*., 2007; *Lowe*, 2011; M. Cassidy et al., Construction of volcanic records from marine sediment cores: A review and case study, Earth-Science Reviews (Montserrat, West Indies), submitted, 2014]. Volcanic material may also reach marine sediments through resedimentation by submarine landslides, seafloor-hugging density-currents, vertical density-currents, and suspension settling in the water column [*Carey*, 1997; *Manville and Wilson*, 2004; *Allen and Freundt*, 2006]. Volcanic-rich submarine landslides that mix with seawater generate long runout turbidity currents whose deposits (turbidites) can provide additional insight into how the landslides were emplaced [*Hunt et al*., 2011, 2013]. Volcanic flank and shelf collapses, mass-wasting events that can be associated with volcanic eruptions, can also create extensive offshore deposits containing large-scale blocks [*Moore et al*., 1994; *Masson et al*., 2006; *Watt et al*., 2012a, 2012b]. The marine sedimentary record around volcanic islands thus provides important clues to past volcanic activity and is often easier to date than the terrestrial record because of weaker erosion and intervening intervals of hemipelagite that can be dated using a variety of techniques (oxygen isotope stratigraphy and AMS radiocarbon dating). Here the term density-current deposit is used to describe deposits that have been emplaced by any form of density or turbidity current. The term eruptive fall deposit is used for tephra fallout that has settled through the water column.

There are few volcanic islands for which we have detailed offshore information on event chronology. Arguably, the most complete offshore data set now comes from the island of Montserrat in the Lesser Antilles. This offshore data set complements unusually detailed subaerial observations of the 1995-recent eruption of the Soufrière Hills volcano [*Druitt and Kokelaar*, 2002; *Wadge et al*., 2014], subsurface magmatic system [e.g., *Paulatto et al*., 2012], and older eruption record [*Harford et al*., 2002; *Smith et al*., 2007], thereby providing a benchmark data set for the evolution of a volcanic island.

Previous research offshore Montserrat has been based on 2-D and 3-D seismic data sets [*Deplus et al*., 2001; *Lebas et al*., 2011; *Watt et al*., 2012a, 2012b; *Crutchley et al*., 2013], repeat multibeam mapping of seafloor bathymetry [*Le Friant et al*., 2008, 2010; *Trofimovs et al*., 2006, 2012], and analysis (Table 1) of short sediment cores [*Le Friant et al*., 2008; *Trofimovs et al*., 2010; *Cassidy*, 2012; *Trofimovs et al*., 2013; *Cassidy et al*., 2013, 2014, Cassidy et al., submitted manuscript, 2014]. In 2012, IODP Expedition 340 added to this benchmark data set by successfully recovering long marine sediment cores at three sites (U1394, U1395, and U1396) offshore of Montserrat (Figure 1). IODP Site U1396 is situated ~33 km to the south west of Montserrat (16°30.49′N, 62°27.10′W; Figure 1) on a topographic high point, 801 mbsl (meters below sea level). Of the three holes cored at Site U1396 (A, B, C), Hole C was the most complete; therefore, we selected this core for high-resolution stratigraphic analysis. Core U1396A was located a few tens of meters away from U1396C and contains similar layers in its uppermost part, allowing correlation of visible layers between U1396A and C. Site U1396 is located away from the expected path of the largest density-current deposits and records a thick sequence of eruptive fall deposit and density-current deposits intercalated with hemipelagic

Table 1. A Summary of Sites Previously Cored Offshore of Montserrat and Data Generated From Core Analysis

Site	Position	Age Coverage (ka)	Stratigraphy	Data Included in Study	Reference
CAR-MON 2	~40 km southwest	~250	Well-defined oxygen isotope stratigraphy	Deposits thought to represent eruptive activity. Abundance of volcanic grain types analyzed in detail, identifying cryptotephra	*Le Friant et al.* [2008]
JC18–19	~52 km southwest	~130	Some AMS dates and low-resolution oxygen isotope stratigraphy	Abundance of volcanic grain types analyzed in detail, identifying cryptotephra. Detailed componentry for each deposit	*Cassidy*[2012] and Cassidy et al. (submitted manuscript, 2014)
JR123-1 to 4	8–13 km south and southwest	110	Some AMS dates	Records of more recent, mainly collapse events. Detailed componentry for each deposit	*Cassidy et al.* [2013, 2014]
JR123-45 to 48	8–13 km south and southeast				
JR123-5 to 44	Up to 30 km to the southeast	110	Well-defined oxygen isotope stratigraphy		*Trofimovs et al.* [2010, 2013]

sediments. The unconsolidated nature of the sediments allowed extended piston coring to be used throughout operations at this site, hence the sedimentary record is relatively undisturbed and complete compared to core material recovered by rotary drilling techniques. This site was cored to study eruption records and links between eruptive activity (recorded at Site U1396) and density-current deposits at adjacent Sites U1394 and U1395 (Figure 1).

Good core recovery at sites U1394 and U1395, situated within the Bouillante-Montserrat Graben (Figure 1), only spans ~250 ka, because these sites lie in a region of high sedimentation rates and are dominated by density-current deposits [*Expedition 340 Scientists*, 2012], including those derived from large submarine

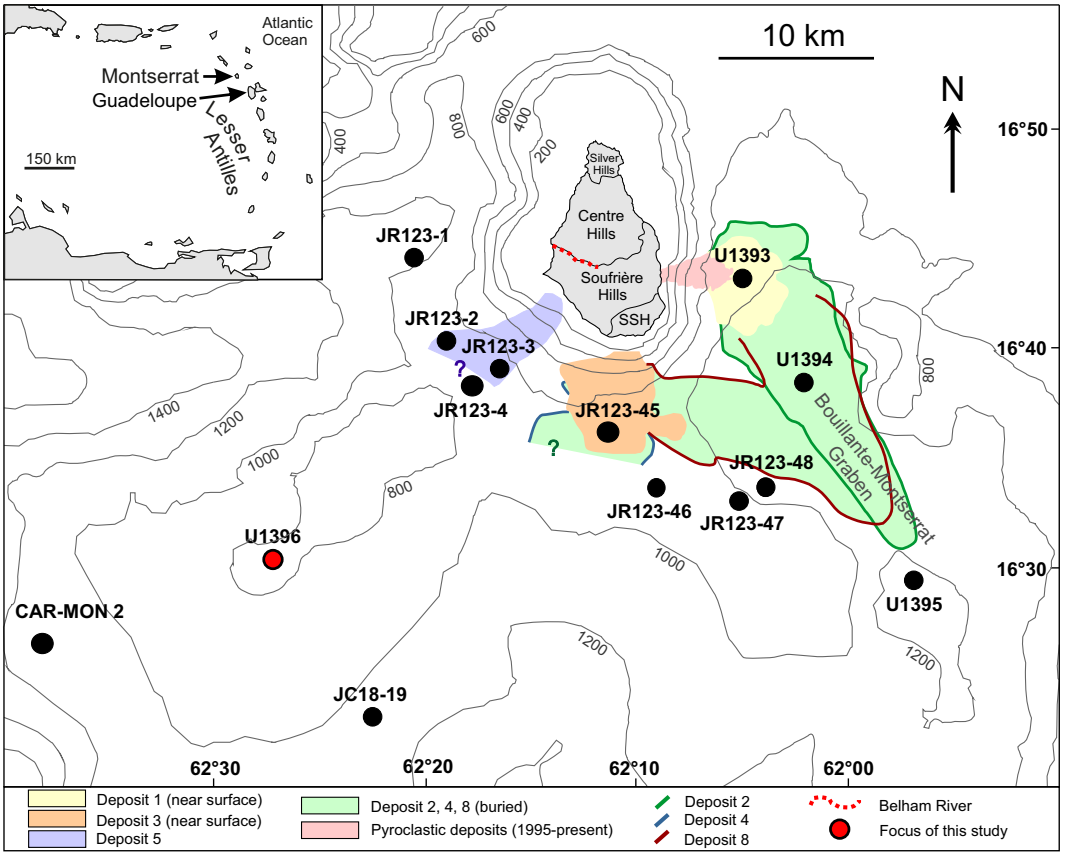

Figure 1. Location of sites drilled during IODP Expedition 340 [*Le Friant et al.*, 2013] and sites previously studied to the south and south west of Montserrat [*Le Friant et al.*, 2008; *Cassidy*, 2012; *Cassidy et al.*, 2013, 2014, Cassidy et al., submitted manuscript, 2014] with outlines of large-scale deposits [*Le Friant et al.*, 2010; *Watt et al.*, 2012a, 2012b]. Lines of bathymetry represent 200 m intervals.

landslides. The presence of large landslide deposits made drilling at these sites difficult, reducing the recovery of material and the drilling depth. Because sites U1394 and U1395 have been subjected to multiple mass-wasting events, they are also likely to contain eroded sections or stratigraphic gaps, which will make it difficult to interpret and date these events. This study, therefore, focuses on the section of Hole U1396C (~250 ka, 7 m) that corresponds to the time span of good core recovery at sites U1394 and U1395. The upper 7 m of U1396C was recovered in full and collected within a single, undisturbed core barrel (U1396C, 1H). This site provides a more complete record of events than U1394 and U1395, including marine tephra fall deposits which form widespread stratigraphic markers and intercalated hemipelagic sediments that can be used to produce an age model.

Prior studies of sediment cores from the south and south west of Montserrat also span ~250 ka [*Le Friant et al*., 2008; *Trofimovs et al*., 2013; *Cassidy et al*., 2013, 2014, Cassidy et al., submitted manuscript, 2014]. These cores have highlighted the complexity of sedimentation and volcanic history in this area, demonstrating that no single site records a comprehensive chronology during this period. For example, two distal sites previously cored within ~15 km of Site U1396 (CAR-MON 2 and JC18–19; Figure 1) contain dissimilar records of eruptive events and density-current deposits [*Le Friant et al*., 2008; Cassidy et al., submitted manuscript, 2014]. Therefore, additional information is necessary to understand the complex history of this area. Here a number of stratigraphic techniques, as well as the identification of distinctive units within the sediments of Site U1396, has allowed the lateral correlation of events to the south and south west of Montserrat [*Le Friant et al*., 2008; *Trofimovs et al*., 2006, 2010, 2012, 2013; *Cassidy et al*., 2013, 2014, Cassidy et al., submitted manuscript, 2014]. This correlation has strengthened the stratigraphy of this area and added a spatial dimension to this data set that will enhance the ability to interpret sites U1394 and U1395 in future research.

The primary goal of this contribution is to establish a robust chronology for the upper 7 m of Site U1396 and to determine the number and ages of visible marine tephra fall deposits and density-current deposits within this interval. The completeness of the record is also assessed by identifying major hiatuses. A secondary goal is to understand the origin of eruptive fall deposits and density-current deposits and the type of event that these deposits record. The chronology of events at Site U1396 is then combined with and compared to previous studies of events during the last 250 ka offshore and onshore Montserrat to improve our understanding of the evolution of this volcanic island.

2. Methodology

2.1. Core Sampling

U1396C was sampled at 5 cm (~0.53–1.79 ka) intervals at the Gulf Coast Core Repository, Texas, USA. Samples for stratigraphic analysis were taken from hemipelagic sediment only, avoiding any obvious disturbance from volcanic input. Sample processing for stratigraphic analysis was carried out at Plymouth University, UK, and sample processing for compositional and grain size analysis was carried out at the National Oceanography Centre, Southampton. Samples were dried in a cool oven at 40°C for 24 h prior to processing to facilitate the removal of fine clay particles. Samples were then rehydrated and immediately washed over a 63 μm sieve. Both the $<$63 and $>$63 μm fractions were collected, filtered, and dried in a cool oven at 40°C for 24 h.

2.2. Oxygen Isotope Stratigraphy

Due to the frequency of density-current and eruptive events recorded at site U1396, oxygen isotope stratigraphy has been chosen as the chief stratigraphic method in this research. Oxygen isotope analyses produce higher resolution dating than biostratigraphy or paleomagnetism during the Pleistocene and can be correlated at a high resolution to global records. Oxygen isotope analyses have been used in combination with AMS radiocarbon dating to identify the magnitude of any hiatuses within the sedimentary record up to the analytical limit of AMS (43.5 ka). Past this age limit, oxygen isotope analyses may not provide sufficient temporal resolution to identify the magnitude of hiatuses; however, it has been possible to identify Marine Isotope Stages (MIS) through comparison to other isotope records from this area. Stable oxygen isotope analysis was carried out at the National Oceanography Centre, Southampton. Twenty specimens of *Globigerinoides ruber* (Figure 2) of size 250–355 μm (~380 μg) were analyzed from each sample using a Europa GEO 20-20 mass spectrometer with an automatic carbonate preparation system (CAPS). Isotope values (δ^{18}O) are

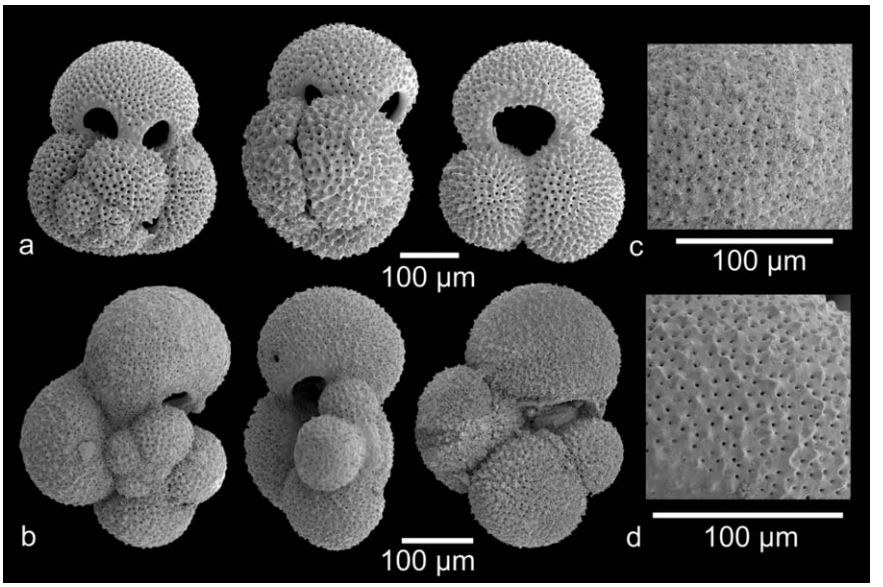

Figure 2. Scanning Electron Microscopy (SEM) images of planktic foraminifera from Hole U1396C. (a) Example of *G. ruber* specimens used for oxygen isotope stratigraphy (0.015 m); (b) Specimens of *G. calida* collected beyond the known species range (220 ka) at ~250 ka (7.005 m); (c) Surface of *G. calida* showing overgrowth (7.005 m); (d) Surface of *G. calida* from the same sample showing no overgrowth (7.005 m).

reported as per mil (‰) deviations of the isotopic ratios ($^{18}O/^{16}O$) calculated to the VPDB scale using an in-house standard calibrated against NBS-19. Analytical reproducibility is 0.065‰ for $\delta^{18}O$.

2.3. AMS Radiocarbon Dating

Three samples in the upper 1.52 m of U1396C were selected for Accelerator Mass Spectrometry (AMS) ^{14}C dating. Analyses were run for samples at 0.455, 0.905, and 1.515 m core depth, situated within the upper extent of hemipelagic sediment. Approximately 1000 specimens (~17 mg) of sonically cleaned *G. ruber* (white and pink) of a size >150 μm were analyzed for each sample. Specimens showing any visual signs of diagenesis or reworking were not used for analysis. Analysis was carried out by Beta Analytic Inc. (Florida, USA) using their in-house protocols (www.radiocarbon.com). Results are reported as conventional radiocarbon years BP, expressed at the $\pm 1\sigma$ level for overall analytical confidence. The AMS dates for 0.455 and 0.905 m have been calibrated against the Marine13 data set using CALIB 7.0 Radiocarbon Calibration Software, which provides ages between 0 and 46.743 ka at 95% probability (2σ). The AMS date for 1.515 m is close to the analytical limit of AMS, thus it is reported as an uncalibrated age of >43.5 ka.

2.4. Biostratigraphy

The revised planktic foraminifera biostratigraphy of *Wade et al*. [2011], calibrated to the geomagnetic polarity time scale of *Cande and Kent* [1995], was followed for this study. All samples were examined for biostratigraphic datum species. For samples showing significant changes in the presence of datum species, a full assemblage of just over 300 specimens was picked from the >150 μm fraction (Table 2).

In addition to planktic foraminifera datum species, the distribution of *Globorotalia menardii* was used to constrain the stratigraphy of U1396. The zonation of *G. menardii* provides a record of climatically induced migration events [*Ericson and Wollin*, 1956; *Reid et al*., 1996] and has been used previously in sediments offshore of Montserrat [*Le Friant et al*., 2008; *Wall-Palmer*, 2013]. Zonal boundaries are defined by points where the abundance of *G. menardii* drops below, or rises above 1% of the planktic foraminifera content [*Le Friant et al*., 2008]. For each sample, 300 planktic foraminifera specimens were counted in the >355 μm fraction to calculate the proportion of *G. menardii* and *Globorotalia tumida*. It was found that, below this size, specimens of *Globorotalia flexuosa* were difficult to distinguish from *G. tumida*. Both *G. menardii* and *G. tumida* were counted because their morphology in the Caribbean Sea is very similar and thus difficult to distinguish. *Wall-Palmer* [2013] showed that combined counts of both species adhere to the zonation published by *Le Friant et al*. [2008].

Table 2. Relative Abundances of Planktic Foraminifera Species Present Throughout the Upper 7 m of U1396C

Depth (mbsf)	*Candeina nitida*	*Globigerina rubescens*	*Globigerinella calida*	*Globigerinella siphonifera*	*Globigerinita glutinata*	*Globigerinoides conglobatus*	*Globigerinoides elongatus*	*Globigerinoides ruber*	*Globigerinoides sacculifer*	*Globigerinoides trilobus*	*Globorotalia crassaformis*	*Globorotalia flexuosa*	*Globorotalia menardii*	*Globorotalia scitula*	*Globorotalia tosaensis*	*Globorotalia truncatulinoides*	*Globorotalia tumida*	*Globorotaloides hexagona*	*Neogloboquadrina dutertrei*	*Orbulina universa*	*Pulleniatina obliquiloculata*	*Sphaeroidinella dehiscens*
0.02	0.3	1.1	1.7	4.8	10.1	1.7	0.8	43.9	9.6	11	0.3	0.3	2.3	0.3	0	1.4	0	0.6	7.6	1.4	0.8	0
0.31	0.6	1	0	4.1	4.1	3.8	3.8	42.4	7.3	10.5	1.3	0	1	0	0	2.2	0.3	0	12.4	2.5	2.5	0
0.41	0	1.5	0	5.4	12.1	1.8	1.8	39.6	5.1	9.3	2.8	0.3	0.8	0.5	0	2.6	0	0	13.9	0.8	1.8	0
6.86	0	0	0.3	9.7	3.6	1.5	0.9	28.2	8.5	7.3	0.9	0.3	0.3	0.3	0	5.5	0	0	29.7	1.2	1.5	0.3
6.91	0	2.5	2.3	6.9	21.2	1.4	3.2	29.3	5.5	6.2	0.9	0	0.5	1.2	0.3	0.6	0	0	15	0	2.8	0

Investigation of calcareous nannofossils within the <63 μm sediment of selected samples was carried out using Scanning Electron Microscopy (SEM). Sediment was fixed to metal stubs using a fine layer of spray adhesive, before being sputter-coated with gold. The calcareous nannofossil zonation *of Kameo and Bralower* [2000] for the Caribbean Sea was used to determine the nannofossil stratigraphy for the core.

2.5. Core Logging

The upper 7 m of Hole U1396C consists of hemipelagic sediments interbedded with a number of volcanic and bioclastic layers of variable thickness. Visual core logs and photographs were used to identify tephra layers within this sequence. Cryptotephras, defined as horizons of ash that are not visible to the naked eye because they are too thin and/or have low concentrations of shards [*Lowe and Hunt*, 2001], are not part of this analysis. Intervals of hemipelagic sediments, between density current deposits or eruptive fall deposits, were identified visually from an elevated fines and carbonate content, as in preceding studies [*Trofimovs et al*., 2006, 2012, 2013]. Shipboard geochemical analysis [*Le Friant et al*., 2013] found that hemipelagic sediments at Site U1396 contain <72 wt % calcium carbonate, indicating that volcanic material makes up at least 25% of background hemipelagic sediment (siliceous biogenic material comprises <2% of the sediment). This is not uncommon for sediments in areas affected by volcanic activity and has been previously noted offshore Montserrat [*Reid et al*., 1996]. Additionally, Cassidy et al. (submitted manuscript, 2014) found that volcaniclastic material made up at least 7% of hemipelagic sediment in core JC18–19. This makes the identification of cryptotephra problematic and given these difficulties, the focus of this study is on macroscopic (visible) event deposits, identified from their color and increased volcanic grain fraction (>40%), with all other sediment treated as hemipelagic material.

2.6. Grain Size and Component Analysis

Grain size was analyzed throughout the upper 7 m of U1396A using dry nested sieves and laser diffraction. For nested sieve analysis, whole samples were placed in a stack of sieves of mesh sizes ranging from -1.5 to 4 phi (2.8–0.063 mm) at 0.5 phi intervals. The percentage of >63 μm material for each sample was calculated during processing by weighing dried samples before and after washing over a 63 μm sieve. For laser-diffraction analysis, samples were left on a shaking table overnight in 25 mL of reverse osmosis water with a 0.05% sodium hexametaphosphate dispersant. Dispersed samples were analyzed using a Malvern (Mastersizer 2000) particle size analyzer (0.2–2000 μm). Accuracy was monitored using standard sized particles (32 and 125 μm) and all samples were run in triplicate.

Component analysis was carried out on >63 μm material. Samples were analyzed from various levels throughout the upper 7 m of U1396A, depending on the unit thickness and grading. A field counting methodology was used, whereby the final values are expressed as a percentage of the total number of grains. For each sample, around 400 individual grains were point-counted and divided into six categories, following the classification of *Le Friant et al.* [2008] and Cassidy et al. (submitted manuscript, 2014). The categories are

(1) vesicular pumiceous clasts; (2) nonvesiculated andesite; (3) altered lithic clasts; (4) crystal and glass fragments; (5) mafic scoria clasts; and (6) bioclasts, which include calcareous microfossils.

3. Results

3.1. Oxygen Isotope Stratigraphy and AMS Radiocarbon Dates

Despite the fragmented record, the isotope profile for Hole U1396C (Figure 3) compares well to published data for this area [*Le Friant et al*., 2008; *Trofimovs et al*., 2010, 2013], as well as the standard planktic oxygen isotope curve constructed from *Imbrie et al*. [1984], *Prell et al*. [1986], and *Martinson et al*. [1987]. Oxygen isotope ratios differ slightly between Hole U1396C and CAR-MON 2, which is likely to be an artifact of differing methodologies. While isotope ratios for Hole U1396C were measured from a single species of planktic foraminifera, isotope ratios for CAR-MON 2 were measured using homogenized <63 μm sediment [*Le Friant et al*., 2008], which contains a high proportion of calcareous nannofossils, as well as juvenile planktic and benthic foraminifera. This difference in methodologies has led to a negative offset in the oxygen isotope record of Hole U1396C, although excursions in both cores are generally of the same magnitude and timing. The oxygen isotope record of Hole U1396C is more comparable to the record of site JR123-35V, situated $\sim$16 km to the north east of Montserrat. This record was also obtained from homogenized <63 μm sediment [*Trofimovs et al*., 2010], but has comparable values to Hole U1396C (Figure 3).

By comparison to the JR123-35V, CAR-MON 2, and standard planktic records, it has been possible to clearly identify MIS boundaries within the upper 7 m of Hole U1396C (Figure 3). Oxygen isotope stratigraphy indicates that the boundary between MIS 7 and MIS 8 lies at 6.705 m in U1396C, dating the base of the study interval at just over 243 ka. Oxygen isotope stratigraphy and AMS radiocarbon dates indicate large variations in the hemipelagic sedimentation rate at Site U1396, ranging between 2.8 cm ka^{-1} in the lower part of the 7 m section studied and $\sim$9.4 cm ka^{-1} at the top of the core (Figure 4). The sedimentation rate at CAR-MON 2 (average 2.3 cm ka^{-1}) is much lower than the sedimentation rate at the top of Hole U1396C, but comparable to the sedimentation rate at 3.7–7 m in Hole U1396C (Figure 4). AMS radiocarbon dates indicate an erosive contact at 0.4 m, where 106–357 cm of sediment has potentially been removed, eroding back to 38 $\pm$ 0.8 ka. This erosion event has removed MIS 1, 2 and part of MIS 3 from the sedimentary record at this site (Figures 3 and 4).

3.2. Biostratigraphy

The planktic foraminifera assemblage throughout the upper 7 m of U1396C is dominated by the subtropical species *Globigerinoides sacculifer*, *Globigerinoides trilobus*, *G. ruber*, *Neogloboquadrina dutertrei*, and *Globigerinita glutinata* (Table 2). Three planktic foraminifera datum species (*Globigerinella calida*, *G. flexuosa*, and *Globorotalia tosaensis*) were identified in the upper 7 m of U1396C. However, the ranges of these species do not adhere to the recently revised datums defined by *Wade et al*. [2011] and, therefore, could not be used for stratigraphic purposes. In U1396C, *G. flexuosa* extends past the defined Last Occurrence (LO) of 70 ka [*Wade et al*., 2011] to the top of the core. This is in agreement with the distribution of *G. flexuosa* within CAR-MON 2 [*Wall-Palmer*, 2013], which extends to $\sim$2 ka. The LO of *G. tosaensis*, reported by *Wade et al*. [2011] as 610 ka, is also extended at Site U1396 to 243–250 ka. Similarly, the First Occurrence (FO) of *G. calida* extends from the defined age of 220 ka [*Wade et al*., 2011] to $>$250 ka, being present in the sediments at 7.005 m (Figure 2) and deeper [*Le Friant et al*., 2013]. This is also consistent with the distribution of planktic foraminifera within CAR-MON 2 [*Wall-Palmer*, 2013] and is known from several other locations [e.g., *Chaisson and Pearson*, 1997]. Overgrowth was also observed on several specimens of *G. calida* at 7.005 m in Hole U1396C (Figure 2) as a result of diagenetic processes. The small number of affected specimens, however, may indicate they have been reworked from an older source. This extended occurrence of stratigraphic datum species requires further work throughout the remainder of Hole U1396C. *Globorotalia flexuosa* is not present within samples from 6.905 to 7.005 m (base of the studied section); however, oxygen isotope stratigraphy suggest that this absence is unlikely to indicate the FO (400 ka), but is rather a response to the environment at the MIS 7/8 boundary. The absence of *G. menardii* in the same samples supports this hypothesis. No other LO or FO data were identified in the upper 7 m of Hole U1396C. *Globorotalia hirsuta* (FO 450 ka), *Globorotalia hessi* (FO 750 ka), and *Globorotalia excelsa* (FO 1 Ma) were not found in any sample, whereas *Globorotalia truncatulinoides* (FO 1.93 Ma) and *Pulleniatina obliquiloculata* (Re-appearance 2.26 Ma) were found throughout the upper 7 m, as expected. Several samples between 6.5 and 7 m in U1396C were

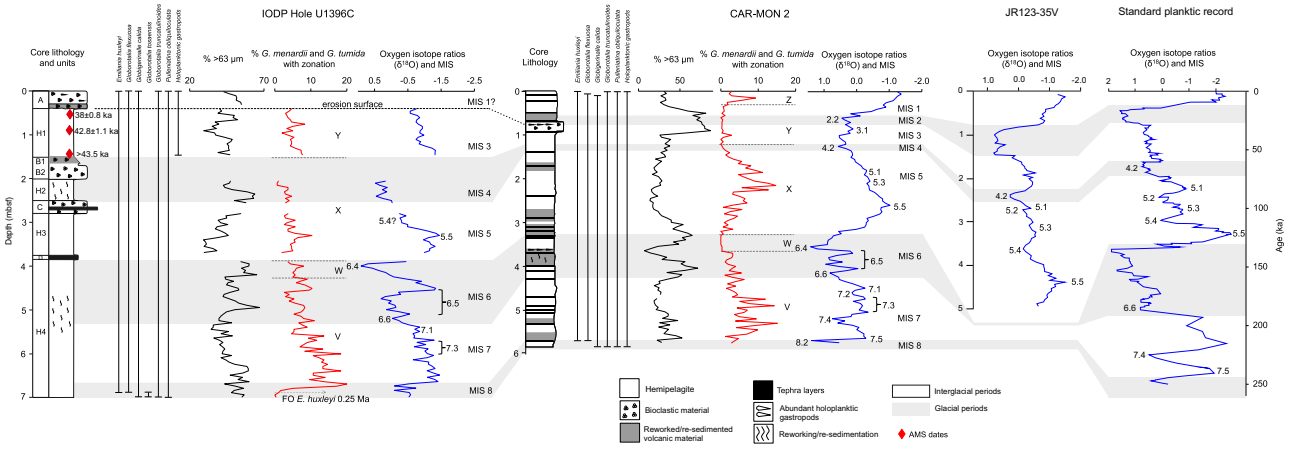

Figure 3. Micropaleontological and geochemical stratigraphy for the upper 7 m of Hole U1396C compared to CAR-MON 2 [*Le Friant et al*., 2008], JR123-35V [*Trofimovs et al*., 2010], and a standard planktic oxygen isotope curve constructed from *Imbrie et al*. [1984], *Prell et al*. [1986], and *Martinson et al*. [1987].

investigated using SEM to locate the FO of the calcareous nannofossil *Emiliania huxleyi* (250 ka). Specimens of *E. huxleyi* were common at 6.905 m, but absent in samples below this. The FO of *E. huxleyi* can therefore be positioned at 6.93 m. No other calcareous nannofossil datum species were found.

Fluctuations of the planktic foraminifera *G. menardii* throughout the upper 7 m of Hole U1396C (Figure 3) do not show a clear definition between the zones identified in CAR-MON 2. Values rarely drop below 1% (zones W and Y) and do not reach the comparably higher values of zones V, X, and Z found in CAR-MON 2 sediments [*Le Friant et al*., 2008]. A single clear zonal boundary can be identified between 6.855 and

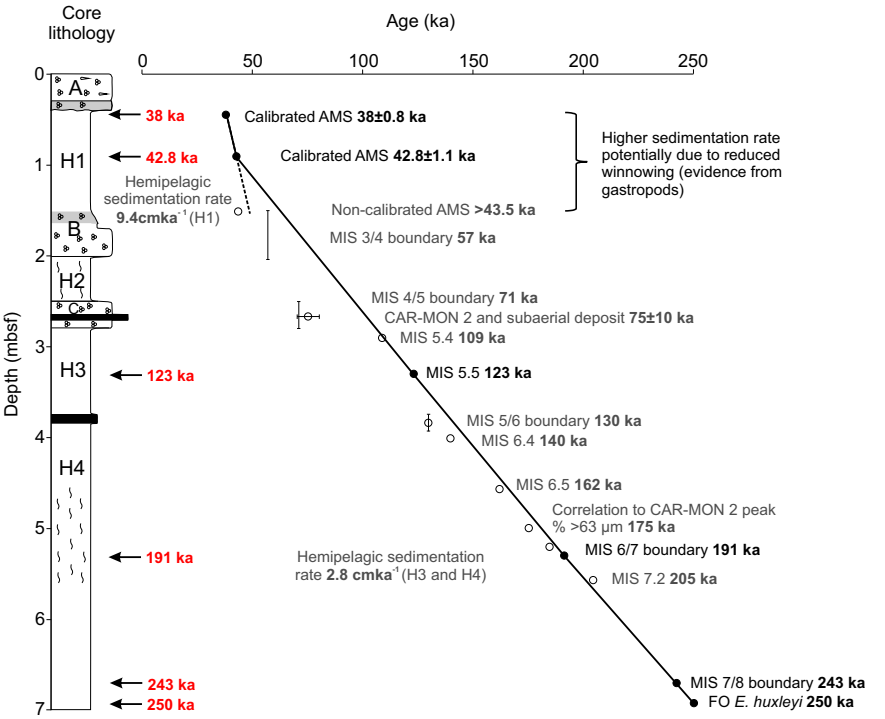

Figure 4. Age-depth plot showing sedimentation rates for the upper 7 m of Hole U1396C. Confident dates are placed along the line as filled points and as red text next to the core lithology. Less confident dates are placed along the line as open circles, with range in age or depth where necessary. See Figure 3 for key to core lithology.

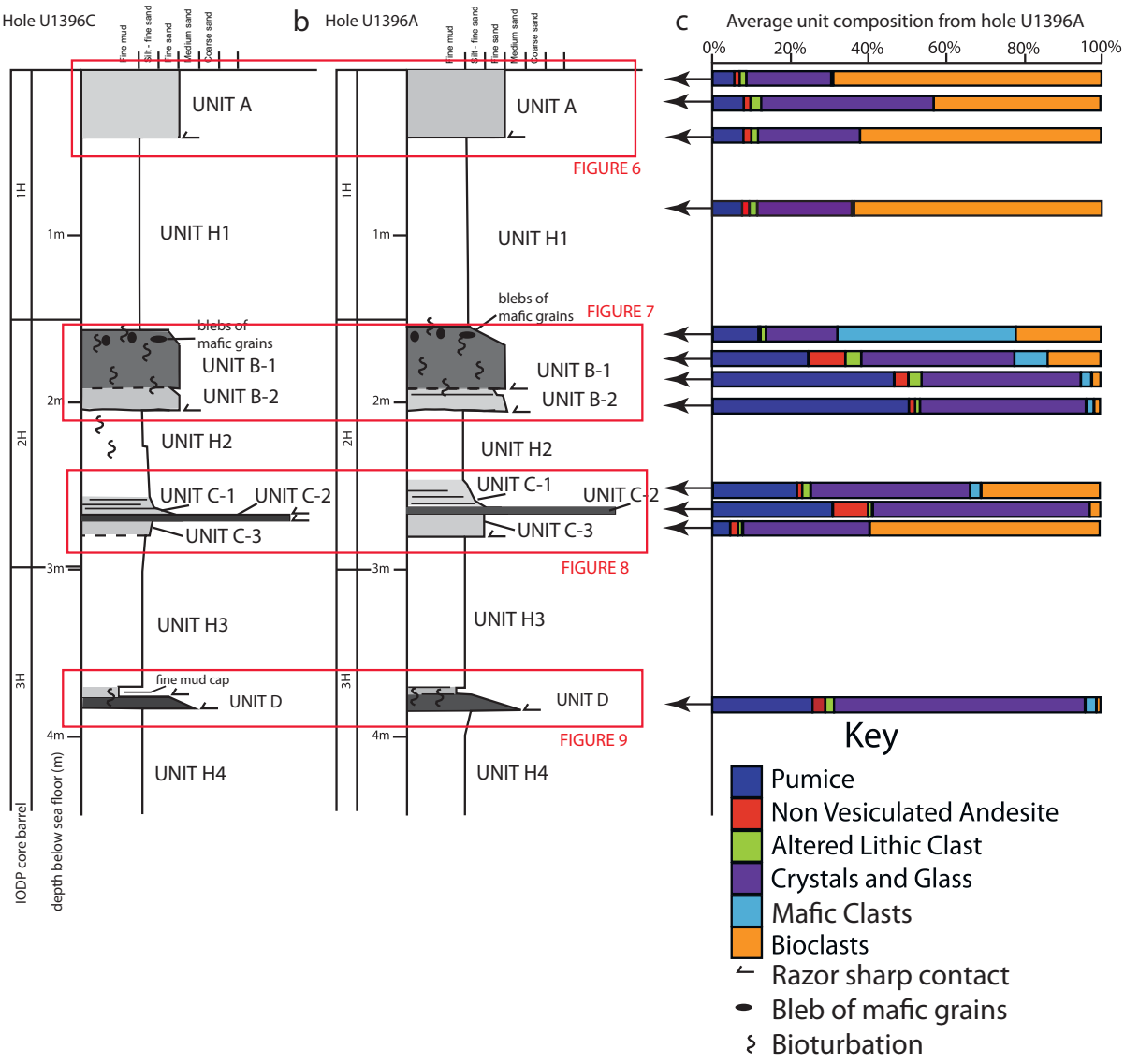

Figure 5. Detailed core logs and correlation of (a) Hole U1396A with (b) Hole U1396C and (c) summary of unit compositions. Red boxes indicate association to more detailed figures.

6.905 m where the abundance of *G. menardii* drops to 0%, representing the transition between MIS 7 and MIS 8.

3.3. Description and Timing of Deposits

3.3.1. Unit A (0–0.400 mbsf), 0–38 ka

Unit A consists of the upper 0.400 m of Hole U1396C immediately below the sea floor and is composed of 50–70% bioclastic material and 30–50% volcaniclastic material (Figures 5 and 6). The bioclastic material is dominated by well-preserved planktic foraminifera and holoplanktic gastropods (pteropods and heteropods). The volcanic component of Unit A is dominated by colorless glass and crystal fragments (feldspars, amphibole, and pyroxene). The mean grain size of Unit A is between 2.5 and 3.1 phi and there is no systematic variation in composition and grain size, or vertical grading (Figure 6 and Table 3). Although the grain size distribution of Unit A is comparable to hemipelagite elsewhere in the core, it is relatively depleted in grain sizes of <63 μm. This, along with a sharp basal contact, suggests the unit is not simply hemipelagite.

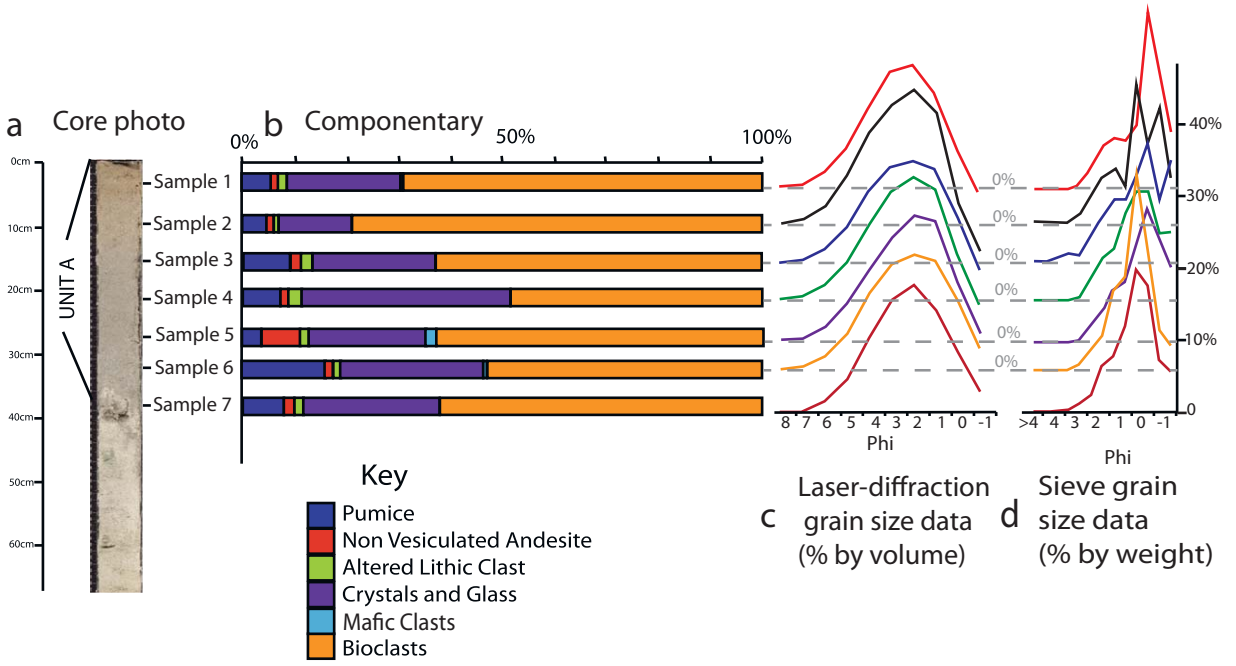

Figure 6. Componentry and grain size analysis of Unit A. (a) Core photo, (b) componentry, (c) laser-diffraction grain size data, and (d) sieve grain size data.

Despite the position of Unit A immediately below the seafloor, geochemical, and biostratigraphical techniques cannot be used to directly date this resedimented deposit, hence the age of Unit A is uncertain. AMS dating at 0.455 m, just below Unit A, produces an age of 38 ± 0.8 ka, which indicates that Unit A was emplaced at any time during the last 38 ± 0.8 ka. This date also indicates a highly erosional contact at the base of this bed, which has removed MIS 1, 2 and the upper ~9 ka of MIS 3 (Figure 3) from the sedimentary record. Assuming the range of hemipelagic sedimentation rates of 2.8–9.6 cm ka^{-1} (Figure 4), approximately 106–357 cm of sediment has been eroded away. This is a major hiatus in the record of Site U1396 and reveals the potential for further large-scale erosion down-core.

3.3.2. Unit H1 (0.400–1.535 mbsf), 38–49.5 ± 1.1 ka

Unit H1 is a hemipelagic unit, with abundant planktic foraminifera and holoplanktic gastropods. It is composed of 55–60% bioclastic material and 40–45% volcaniclastic material (Figure 7), with a mean grain size of 3.3–3.9 phi. Oxygen isotope stratigraphy and AMS radiocarbon dating (0.455 m: 38 ± 0.8 ka, 0.905 m: 42.8 ± 1.1 ka, 1.515 m: >43.5 ka) indicate that Unit H1 is positioned with MIS 3. The average sedimentation rate (9.4 cm ka^{-1}; Figure 4) can be used to date this deposit as 38–49.5 ± 1.1 ka.

3.3.3. Unit B (1.535–2.040 mbsf), 49.5 ± 1.1–71 ka

Unit B has a sharp basal surface and is composed of 60–98% volcaniclastic material and 2–40% bioclastic material (Figures 5 and 7). The unit comprises two compositionally distinct parts (B1, 1.535–1.700 mbsf and B2, 1.700–2.040 mbsf), both of which are subtly normally graded and generally not well sorted (Table 3 and Figure 7). The lower part of the unit (B2) is richer in bioclastic grains, giving it a lighter hue, and sometimes lacks mafic grains (Figure 7). This bioclastic material includes rare fragments of shallow water benthic foraminifera, suggesting transport from a shallow water area. The upper part of the unit (B1) contains a greater abundance of mafic grains, and fewer bioclastic grains. Holoplanktic gastropod shells are not present within Unit B or any of the sediments below.

The age of this unit is difficult to constrain because the planktic foraminifera within the unit (necessary for oxygen isotope analysis) are all likely to be reworked or resedimented and would not produce an accurate date for the deposit. However, average sedimentation rates and oxygen isotope stratigraphy broadly date Unit B as 49.5 ± 1.1–71 ka.

Table 3. Inman Sorting Coefficients [Inman, 1952] for All Samples Analyzed for Clast Componentry

Sample	Sample Number (Figures 6–9)	phi 16	phi 84	Inman Sorting Coefficient
96A1H1W27/27.5	1	5.5	1.5	2
96A1H1W3/3.5	2	5.5	1.5	2
96A1H1W9/9.5	3	5.5	1.5	2
96A1H1W15/15.5	4	5.5	1.5	2
96A1H1W21/21.5	5	5.5	1.5	2
96A1H1W32/32.5	6	5.5	0.5	2.5
96A1H1W38/38.5	7	5.5	0.5	2.5
96A1H1W45/46	8	6.5	1.5	2.5
96A1H1W90/91	9	7.5	1.5	3
96A1H2W1.5/2.5	10	7.5	2.5	2.5
96A1H2W28/28.5	11	3.5	0.5	1.5
96A1H2W34/34.5	12	3.5	1.5	1
96A1H2W38.5/39	13	6.5	2.5	2
96A1H2W41/41.5	14	4.5	1.5	1.5
96A1H2W46/46.5	15	3.5	1.5	1
96A1H2W52/53	16	6.5	2.5	2
96A1H2W98/99	17	6.5	2.5	2
96A1H2W110/110.5	18	2.5	0.5	1
96A1H2W113/113.5	19	3.5	0.5	1.5
96A1H2W113/114	20	2.5	0.5	1

3.3.4. Unit H2 (2.040–2.500 mbsf), 57–71 ka

Unit H2 is composed of hemipelagic sediments containing reworked volcanic material. Individual volcanic events cannot be identified within this unit due to a high background content of volcanic clasts. Oxygen isotope stratigraphy indicates that Unit H2 is within MIS 4, which dates the unit as 57–71 ka (Figure 3).

3.3.5. Unit C (2.500–2.780 mbsf), 57–105 ka

Unit C comprises three distinct layers without intervening hemipelagite (Figures 5 and 8). The uppermost interval (Unit C1, 2.500–2.650 mbsf) is made up of 30–35% bioclastic material, and 65–70% volcaniclastic material, including abundant pumice clasts (20–25%; Figure 8). There is evidence of bioturbation at the top of Unit C1 and a number of planar laminae visible throughout. These structures are highlighted by variations in crystal and pumice content. Unit C2 (2.650–2.690 mbsf) is distinctly coarser than either Units C1 or C3. It is made up of >95% volcanic clasts, including 33% pumice and 54% glass and crystal fragments (Figure 8). Unit C3 (2.690–2.780 mbsf) is bioclast-rich, with 60–68% bioclastic material and 32–40% volcaniclastic material (dominantly glass and crystal fragments). The grain size distribution of Unit C3 is comparable to hemipelagite elsewhere in the core, but is relatively depleted in grain sizes of <63 μm. Unit C3 does not have a distinct base, and it grades into underlying hemipelagite within H3.

Oxygen isotope stratigraphy of overlying and underlying hemipelagic sediment suggest that Unit C was deposited during the transition from MIS 5 to MIS 4, more accurately, between MIS 5.4 and the MIS 3/4 boundary, giving an age of 57–109 ka. The base of Unit C3 can be dated as ~105 ka using the average sedimentation rate (2.8 cm ka^{-1}) of hemipelagite above MIS 5.4, constraining the age of Unit C as 57–105 ka.

3.3.6. Unit H3 (2.780–3.705 mbsf), 71–130 ka

Unit H3 is composed of hemipelagic sediment with abundant planktic foraminifera. Some color variations can be seen within the unit. Oxygen isotope stratigraphy indicates that Unit H3 is within MIS 5, with MIS 5.5 (123 ka) present at 3.305 m and the MIS 5/6 boundary below Unit H3 (Figure 3). This dates the deposit to 71–130 ka, with 123 ka at 3.305 m. Although volcanic material was not visible as macroscopic layers within Unit H3, or identified during micropaleontological analysis, oxygen isotope data suggest a high sedimentation rate between MIS 5.5 and the MIS 5/6 boundary (Figure 4). This may indicate the presence of cryptotephras with Unit H3.

3.3.7. Unit D (3.705–3.835 mbsf), 123–140 ka (~130 ka)

Unit D is made up of >95% volcaniclastic material, including 60% glass and crystal fragments, 25% pumice, and ~5% mafic material (Figures 5 and 9). It is normally graded (Figure 9) with some evidence of bioturbation at the top and is capped by a fine mud. The age of Unit D is relatively well constrained to be between MIS 5.5 (123 ka) in H3 and MIS 6.4 (140 ka) in H4. Unit D appears to directly overlie the MIS 5/6 boundary at 130 ka, dating the unit as ~130 ka.

3.3.8. Unit H4 (3.835–7.000 mbsf), 130–250 ka

The upper part of Unit H4 (3.835–4.550 m) is composed of hemipelagic sediment with abundant planktic foraminifera. The middle part of H4 (4.550–5.590 m) is composed of hemipelagic sediment with more abundant volcanic clasts. Intense bioturbation has reworked the volcanic material, making it impossible to identify individual events. The lower part of Unit H4 (5.590–7.000 m) is composed of

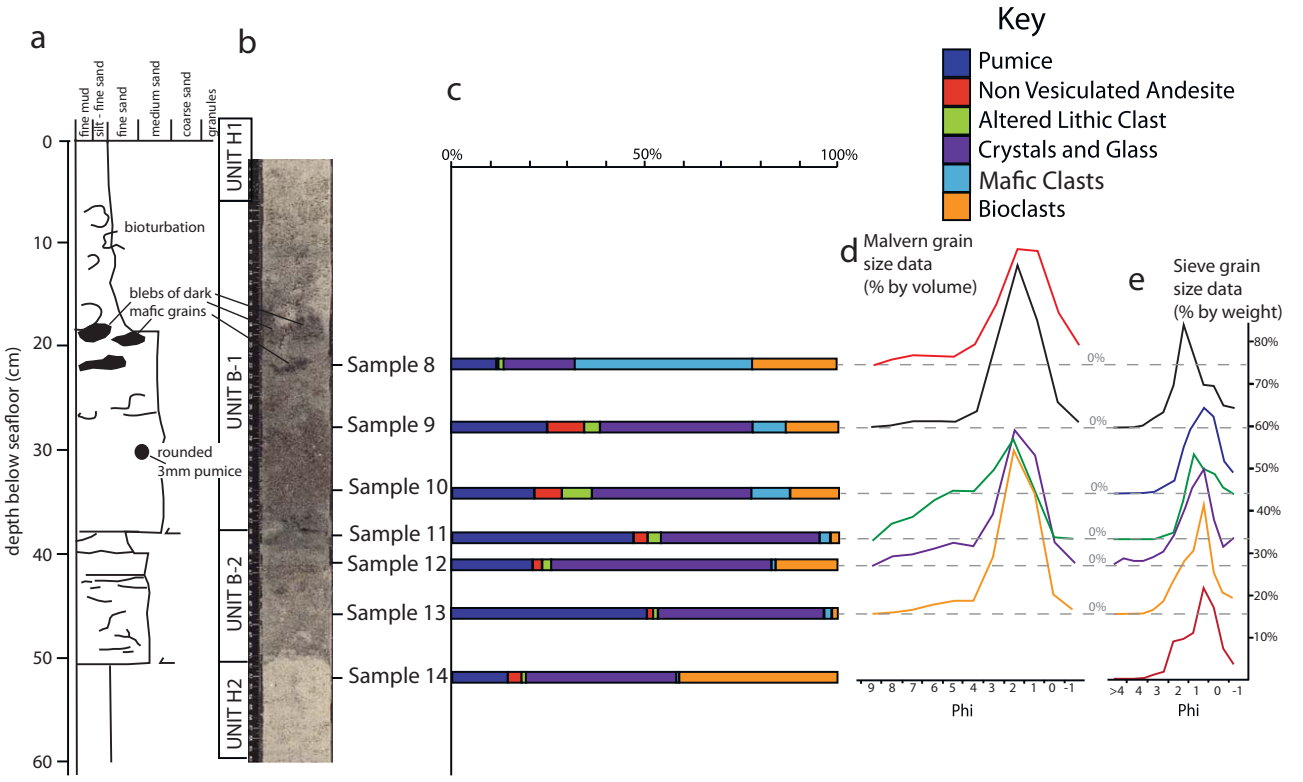

Figure 7. Componentry and grain size analysis of Unit B (subunits B1 and B2). (a) Graphic core log, (b) core photo, (c) componentry, (d) laser-diffraction grain size data, and (e) sieve grain size data.

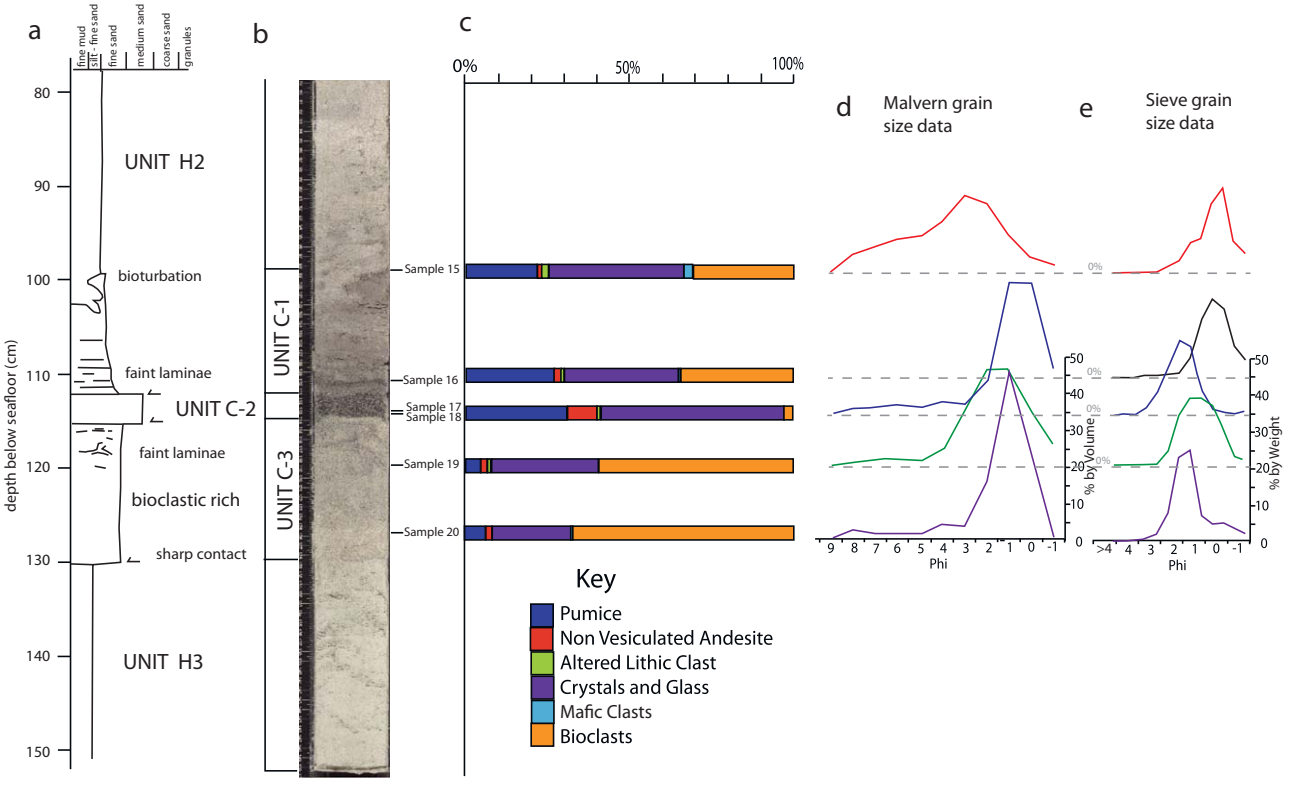

Figure 8. Componentry and grain size analysis of Unit C (subunits C1–C3). (a) Graphic core log, (b) core photo, (c) componentry, (d) laser-diffraction grain size data, and (e) sieve grain size data.

hemipelagic sediment with abundant planktic foraminifera and a reduced volcaniclastic component. A number of stratigraphic markers are present within Unit H4. The top of the unit can be dated as ~130 ka by the MIS 5/6 boundary and the base of the unit can be dated by the FO of *E. huxleyi* at 250 ka (6.930 m).

4. Discussion

4.1. Bottom Water Currents at Site U1396C

The organic carbon content of U1396 is quite low, generally <0.2% (0.13 ± 0.05%, n = 27; J. McManus, personal communication, 2014). These values are typical of other oligotrophic ocean regions of the tropical/subtropical Atlantic [*Ziebis et al*., 2012], but may be partly influenced by the removal of fine-grained sediment by bottom water currents. Strong bottom currents have been observed during previous research cruises in the same topographically high area, and it is likely that these contributed to the differences in microfossil content between Hole U1396C and CAR-MON 2. In addition to differences in the abundance of *G. menardii*, which is not expected from two sites situated so close together, the delicate aragonite shells of holoplanktic gastropods, which are found throughout CAR-MON 2 [*Wall-Palmer et al*., 2013] and at IODP sites U1394 and U1395 [*Expedition 340 Scientists*, 2012], are absent from U1396C sediments below the upper 1.5 m and from nearby site JC18–19 below the upper 0.95 m. Holoplanktic gastropod shells have a low mass and their large aperture makes them easily transported by currents. Because aragonitic holoplanktic gastropods are abundant throughout CAR-MON 2, which was collected at 1102 mbsl, their absence in U1396C and JC18–19 cannot be due to aragonite dissolution, because Site U1396C is situated in shallower water. This suggests that winnowing from strong currents has also removed the less dense holoplanktic gastropods. Evidence for winnowing is further supported by differences in grain size between the two sites. In general, samples from Site U1396 contain a higher percentage of coarse (>63 μm) sediment than CAR-MON 2, suggesting that fine sediment has been removed from Site U1396 (Figure 3). Some CAR-MON 2 sediments contain a high proportion of coarse material; however, upon further investigation, it is apparent that this coarse material is made up of large planktic foraminifera and holoplanktic gastropods and is thus, not directly comparable to the coarse sediment in Hole U1396C. These observations strongly suggest that parts of the sedimentary record at Site U1396 were affected by strong bottom water currents, potentially modifying their grain size distribution and bed thickness. Winnowing has not previously been noticed in sediments offshore Montserrat, so further investigation is required to understand whether these currents are related to the proximity of gullies and other topographic features. The position and extent of such currents may help to determine future sampling sites in this area.

4.2. Distinguishing Eruptive Fall Deposits From Density-Current Deposits

The depositional mechanisms of volcaniclastic material in marine sediments are often ambiguous, making it difficult to distinguish between eruption fall deposits and density-current deposits [*Manville and Wilson*, 2004]. Settling through the water column, bioturbation and the influence of bottom currents can all affect the sorting, grading, and componentry characteristics of fall deposits, which result in similarities to volcaniclast-rich density-current deposits [*Carey*, 1997; *Manville and Wilson*, 2004]. Thus, there remain ambiguities to deposit interpretation which even detailed investigations of grain morphology or petrological characteristics may not fully resolve. However, in spite of these caveats, we observe two broad deposit types that can be differentiated in terms of their bioclastic component and, to a lesser degree, their sorting. We interpret deposits with fewer than 5% bioclasts, which are relatively well sorted, tend to have a sharp base, but lack evidence for basal erosion and internal tractional structures, as most likely to derive from eruption fallout. All other units rich in volcanic clasts (41–95%), with abundant bioclasts (5–59%), which often display tractional structures and erosive boundaries, are interpreted as most likely representing seafloor-hugging density-currents derived from other processes, which may still represent volcanic events (e.g., entry of pyroclastic density-currents to the marine environment). Following this criteria, we recognize five density-current deposits (Units A, B1, B2, C1, and C3), one fall deposit (C2), and one unit which is difficult to interpret (D) within Hole U1396C. As outlined above, we reiterate that these criteria remain interpretations, and are not fully conclusive.

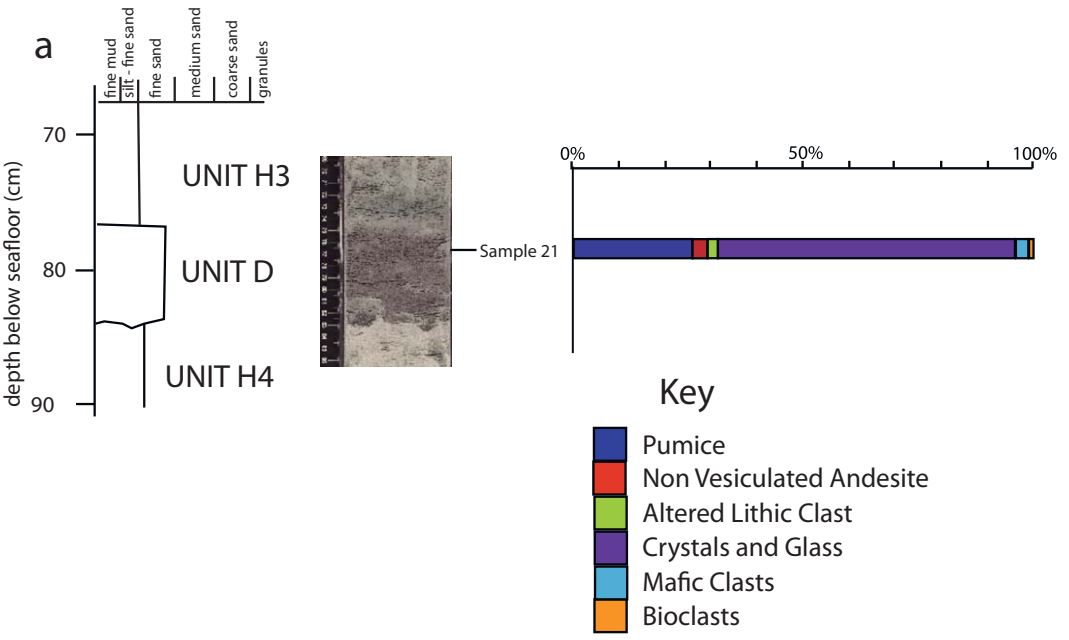

Figure 9. Componentry analysis of Unit D. (a) Graphic core log, (b) core photo, and (c) componentry.

4.3. Combined Chronology of the South and South West of Montserrat

4.3.1. Small-Scale Events 147–250 ka

During the period 147–250 ka, Site U1396 does not preserve any of the visible tephra layers that have been identified at CAR-MON 2 (Figures 10 and 11). This is unexpected because Site U1396 lies directly between Soufrière Hills and CAR-MON 2, implying that any sediment input from Soufrière Hills (airborne or water-transported) reaching CAR-MON 2 passed straight over Site U1396. It is likely that volcanic material from this activity was initially deposited at Site U1396, but was subsequently partially bioturbated to leave cryptotephras that cannot be seen by the naked eye. Intense bioturbation was identified in CAR-MON 2 between 162 and 175 ka and corresponding bioturbation was also observed in Hole U1396C. It can be assumed that eruptive fall deposits and density-current deposits at Site U1396 from ~147 ka to ~250 ka were smaller in scale than during some later time periods or that material from these events did not reach Site U1396.

4.3.2. Overlapping Activity Soufrière Hills and South Soufrière Hills 124–147 ka

During this period, distal sites U1396C, CAR-MON 2, and JC18–19 preserve volcanic material from the Soufrière Hills, intercalated with distinctive mafic clasts, consistent with the composition of subaerial material from the South Soufrière Hills volcanic center [*Harford et al*., 2002; *Le Friant et al*., 2008; *Cassidy* 2012; *Cassidy et al*., 2014]. At ~130 ka, Hole U1396C records this activity as a single, glass, and crystal-rich layer (Unit D), with a low proportion of mafic material. This unit shows characteristics of both an eruptive fall deposit and a density-current deposit, hence the depositional process could not be interpreted. At ~130 ka a similar glass and crystal-rich volcanic layer with a low proportion of mafic material is recorded within JC18–19 [*Cassidy*, 2012] and a number of mafic-rich volcanic deposits are also preserved within CAR-MON 2 at 124–147 ka [*Le Friant et al*., 2008]. These deposits correlate both in timing and composition with the overlapping Soufrière Hills and South Soufrière Hills eruptive activity. Subaerial South Soufrière Hills deposits have been Ar-Ar dated as 128–131 ka [*Harford et al*., 2002]. The depositional processes of these units are unclear and may represent reworked marine tephra fall deposits or the distal toes of large-scale density-current deposits (Deposit 2; Figure 1) that have been linked to this period of activity [*Lebas et al*., 2011; *Watt et al*., 2012a, 2012b].

4.3.3. Flank Collapses of Subaerial South Soufrière Hills Deposits 103–110 ka

The low number of volcaniclastic units observed across all sites suggest that this was a dormant period on Montserrat, which follows similar interpretations from the subaerial record [*Smith et al*., 2007]. During this

quiescent period, a number of flank collapses to the south of Montserrat caused subaerial South Soufrière Hills deposits to enter the proximal waters as density-currents [*Cassidy et al*., 2014]. This distinctive, mafic-rich material is recorded in all of the south and south west JR123 cores (except JR123-3, which is too shallow; Figure 10), as well as along the Bouillante-Montserrat Graben, to the south east [*Trofimovs et al*., 2013]. These collapse deposits have been dated at 103–110 ka [*Trofimovs et al*., 2013] and occurred in stages, as indicated by a gap of ~2 ka between an upper and lower deposit [*Cassidy et al*., 2014]. The collapse deposits may also be associated with Deposit 3 (Figure 1), a major (~1.3 km^3) blocky debris avalanche deposit identified by seismic surveys to the south of Montserrat [*Le Friant et al*., 2004; *Lebas et al*., 2011; *Watt et al*., 2012b]. Such a large-scale collapse and the resulting density-current is likely to have reached Site U1396C. The timing of Unit C3 (~105 ka) coincides with the large-scale collapses, but is relatively lacking in mafic clasts when compared to the mafic-rich units identified in the JR123 cores. However, the long distance traveled by this density-current would have increased the bioclastic content of the deposit, and flow processes may have caused progressive loss of denser mafic grains with distance from shore. Thus, Unit C3 may be related to Deposit 3 (Figures 10 and 11).

4.3.4. Heightened Activity of Soufrière Hills 75 ± 10 ka

At this time, many of the sites to the south and south west of Montserrat indicate strong eruptive activity from Soufrière Hills, with subsequent volcanic collapses (Figures 10 and 11). At Site U1396, the lack of hemipelagic material between units C1 and C3 suggest that mass flows occurred immediately prior to and following eruptive activity at ~105 ka. However, it is also possible that these events occurred independently of each other and that erosion has removed any original intervening hemipelagic sediment. Marine tephra fallout within Unit C2 is rich in glass and crystal fragments and comparable to the composition of a marine tephra layer within CAR-MON 2, dated at 77 ka (Figure 10) and similar deposits within JC18–19 and JR123-2 [*Le Friant et al*., 2008; *Cassidy*, 2012], as well as within the subaerial record [*Harford et al*., 2002]. *Harford et al*. [2002] Ar-Ar dated this event in the subaerial record at 75 ± 10 ka. The spatial extent of this deposit suggests a major explosive eruption. This activity was closely followed by deposition from a stratified volcaniclastic density-current deposit, shown by the internal laminations and flow structures within Hole U1396C (Unit C1) and JR123-1 and 2. This unit was described by *Cassidy* [2012] as being deposited by a low-concentration turbidity current with similar components and clast morphologies to lahar deposits from the Belham River Valley, to the west of Montserrat (Figure 1). The geographical position of Site U1396, JC18–19, JR123-1 and 2 supports this source for the density-current deposit (Figure 1). This density-current potentially reached CAR-MON 2, in which reworked volcaniclastic material directly overlies the 77 ka event [*Le Friant et al*., 2008].

4.3.5. Mafic and Bioclast-Rich Density-Currents From Shallow Waters 30–50 ka

This period represents an episode of strong sedimentation by density-currents, incorporating material from both Soufrière Hills and South Soufrière Hills, as recorded at Hole U1396C (49.5 ± 1.1 ka, Unit B; Figure 10). These events are preserved as mixed bioclast-rich volcaniclastic deposits, containing mafic material and occurring in more than one stage. Fossils of shallow water organisms within this deposit suggest that material was transported through the island shelf. Unit B1 also contains pods of distinctive mafic scoria clasts and differs from the overlying sediment by the absence of holoplanktic gastropods. A comparable deposit, containing mafic clasts and marking the disappearance of holoplanktic gastropods has been described in JC18–19 (Cassidy et al., submitted manuscript, 2014). In common with Site U1396, AMS dating of JC18–19 suggests that this was a period of high sedimentation rates (Figure 10) with a number of deposits preserved from 40.5 ± 1.1 to 42.1 ± 0.8 [*Cassidy*, 2012]. At JR123-2 and 3, similar bioclastic and volcanic clast-rich deposits containing mafic material have been described by *Cassidy et al*. [2013] as the relatively small (0.3 km^3) submarine landslide identified as Deposit 5 (Figure 1) by *Lebas et al*. [2011]. However, *Cassidy et al*. [2013] suggest that this deposit was associated with, and is of a similar age to, a high-energy density-current deposit dated as 8–12 ka which is positioned directly above (JR123-2 and 3; Figure 10). The lack of intervening hemipelagic sediment between the two deposits in JR123-2 and 3 means that accurate AMS dating of the lower unit (Deposit 5) is not possible. Several depositional scenarios were presented by *Cassidy et al*. [2013], all of which indicating that the two deposits are of a similar age. However, it is also possible that the underlying Deposit 5 was emplaced much earlier (~43 ka; Figure 10) and that the more recent 8–12 ka density-current eroded into it later. This is not unlikely because the 8–12 ka event was highly erosive. It is, therefore, possible that Deposit 5 is associated with the bioclast-rich volcaniclastic deposits at sites U1396 and JC18–19. The source of mafic material within these multistage density current deposits may

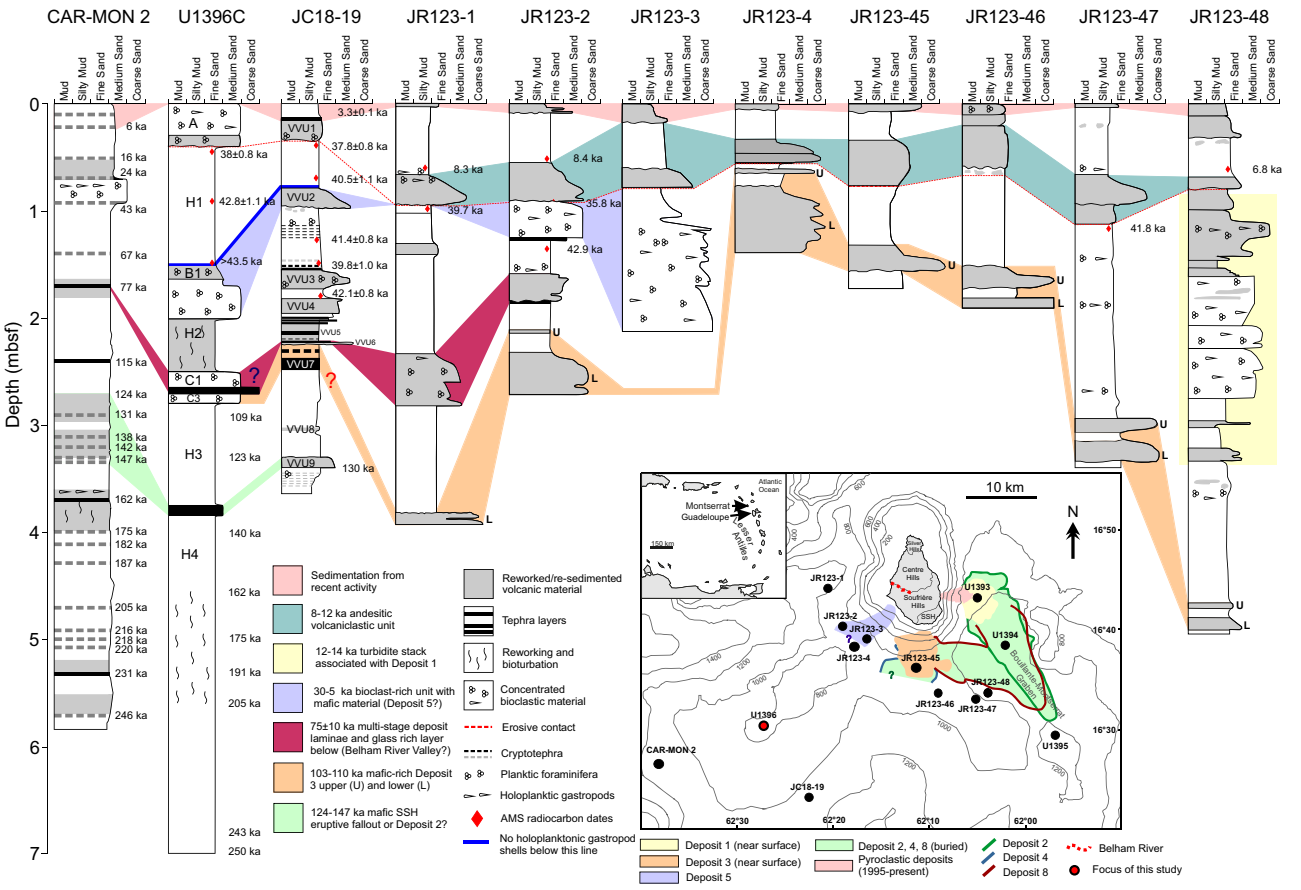

Figure 10. Stratigraphic logs for cores recovered from the south and south west of Montserrat with correlated events. Inset map shows the geographical positions of coring sites. Partially modified from *Le Friant et al.* [2008], *Cassidy* [2012], *Trofimovs et al.* [2013], *Cassidy et al.* [2013, 2014, Cassidy et al., submitted manuscript, 2014].

have originated from the erosion of previous flank collapses of subaerial South Soufrière Hills deposits (Deposit 3, 103–110 ka). However, it may also have originated from contemporaneous eruptive activity. A subaerial deposit containing a comparable minor mafic component has been Ar-Ar dated at 38 ± 8 ka [*Harford et al.*, 2002].

4.3.6. Large-Scale Deposits and Erosion 8–14 ka

Sediments offshore of Montserrat record two major events during this period. The first is a large-scale density current deposit, produced by a carbonate platform failure at 12–14 ka [*Trofimovs et al.*, 2010, 2013]. This powerful event deposited a thick stack of bioclast-rich (containing shallow water fauna) volcaniclastic deposits within the Bouillante-Montserrat Graben (Deposit 1; Figures 10 and 11). These deposits are not preserved at any of the sites to the south west of Montserrat, which is probably due to subsequent removal by erosion which occurred at 8–12 ka, during the second major event. All of the sites to the south and south west, including Site U1396, record an irregular erosion surface (~35 to ~42 ka; Figure 10) linked to sedimentation from the passage of a high-energy density-current, which occurred at 8–12 ka [*Cassidy et al.*, 2013]. Site U1396 reveals that this was a powerful density-current, capable of eroding up to 106–357 cm 33 km offshore. At proximal sites (Figures 10 and 11), this unit is interpreted as being derived from one, or several, primary andesitic volcaniclastic deposits, originating from the south west of Montserrat and transported by turbidity currents [*Cassidy et al.*, 2013]. The thick, proximal, coarse-grained deposits become finer-grained and richer in bioclats at distal site JC18–19. However, at Site U1396, the erosional surface is overlain by the bioclastic-rich Unit A (Figure 10), rather than a volcaniclastic deposit. The process of deposition for Unit A is difficult to interpret because, despite the high bioclastic content, the low proportion of fine grain size material suggests that it is not merely composed of hemipelagic sediment (Figures 6–8). This indicates that Unit A was formed either by resuspension, resedimentation

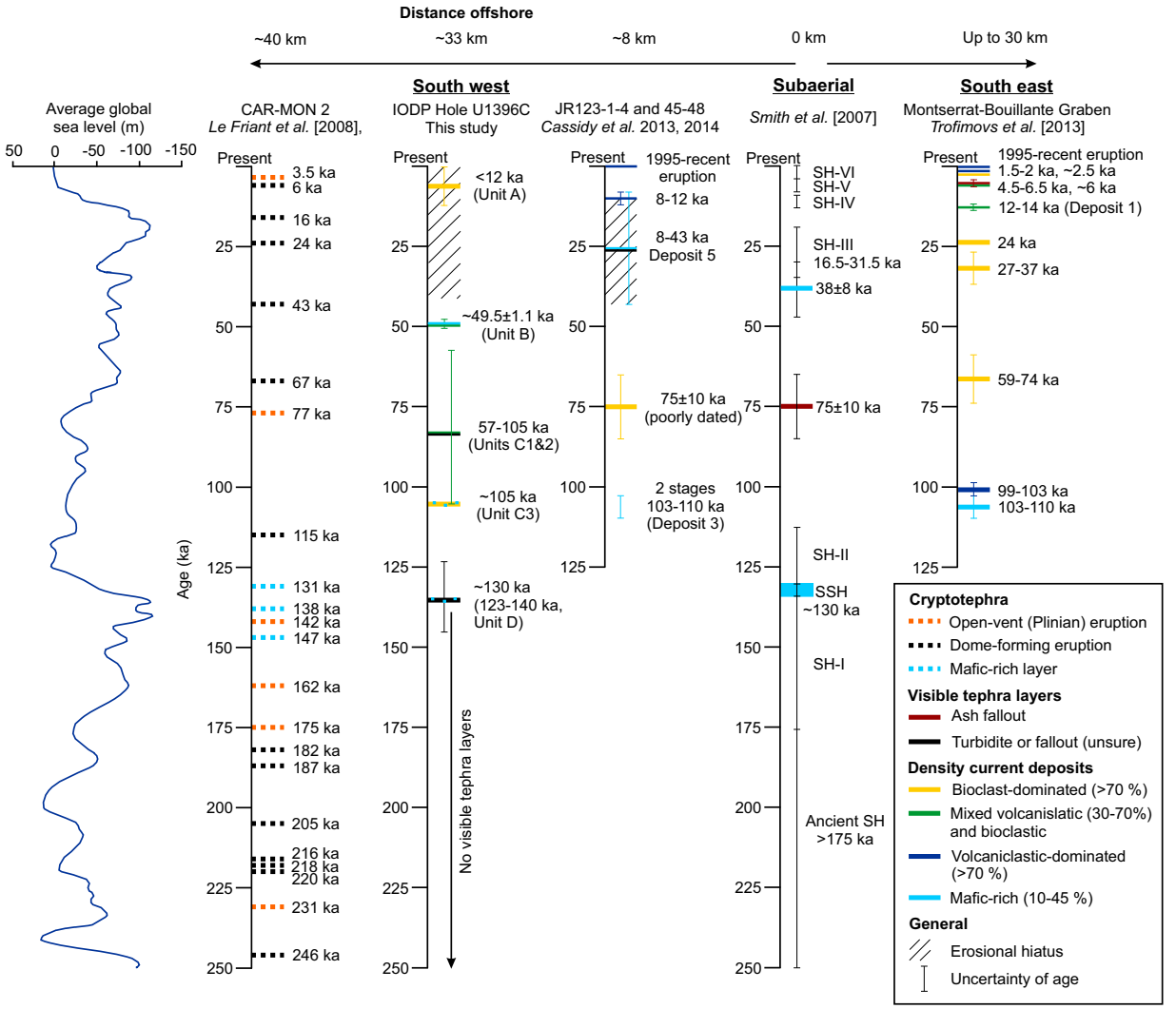

Figure 11. Comparison of dated subaerial sequences of Soufrière Hills and South Soufrière Hills [*Harford et al.*, 2002; *Smith et al.*, 2007], tephrochronology from the south east offshore of Montserrat [*Trofimovs et al.*, 2013] and from the south west offshore of Montserrat [*Le Friant et al.*, 2008; *Cassidy et al.*, 2013, 2014, also Cassidy et al., submitted manuscript, 2014], including the tephrochronology from this study. Average global sea level curve from *Lea et al.* [2002].

(transportation by density-currents), or by winnowing by strong currents. Although winnowing of the sediment by bottom water currents, which could remove fine material, has been detected in Hole U1396C, the abundant holoplanktic gastropods within Unit A indicate that winnowing has not affected this deposit. In addition, the lack of internal structures within Unit A indicates that it was deposited by a single event. Therefore, Unit A was most likely produced by the resuspension or resedimentation of material, leading to two hypotheses.

4.3.7. The Origin of Unit A 0–12 ka

The first hypothesis is that Unit A is was formed by a low-density submarine current (or submarine-surge) originating from a pyroclastic flow and associated with the 8–12 ka event. In this scenario, submarine surge from the 8–12 ka density-current eroded deeply into the sediment surface at Site U1396, resuspending bioclast-rich sediments, which then settled back on top, forming Unit A. This is a feasible mechanism for deposition. However, the average sedimentation rate at this site suggests that 22–32 cm of hemipelagic drape should lie above Unit A. The lack of this drape is not an artifact of coring, because deposits similar to Unit A, with no overlying drape, have recently been collected by multicoring (that captures the sediment-water interface) in the same topographically high area during the JC83 cruise. Rather, the lack of drape may be explained by increased intensity of bottom water currents following the deposition of Unit A, which

would have constantly mixed or removed the hemipelagic drape. However, it is expected that this scenario would still lead to some buildup of drape above Unit A.

A second hypothesis for the origin of Unit A is that it formed more recently by density-currents produced by the ongoing eruptive activity of Soufrière Hills. The series of major recent eruptions of Soufrière Hills [*Trofimovs et al*., 2013] may have been capable of eroding hemipelagic drape at Site U1396 back to the 8–12 ka erosional surface, and potentially eroding further into the sedimentary record and finally depositing the bioclast-rich layer, Unit A. These events potentially include a particularly violent pyroclastic surge following failure of a crater rim on Boxing Day 1997 [*Sparks et al*., 2002]. Such recent, large-scale erosion has been observed at proximal sites within the Bouillante-Montserrat Graben [*Trofimovs et al*., 2013]. However, if this mechanism produced Unit A, similar erosion and bioclast-rich deposits would be expected at other sites around Site U1396, in particular JC18–19. Therefore, no hypothesis satisfactorily explains all of the observations, and Unit A is likely to have been produced by a combination of factors. Further analysis of newly collected material (JC83) may provide more clues to the mechanisms of deposition.

4.4. Association Between Eruptive Activity and Collapses to the South and South West

Although two of the four volcaniclastic units within Hole U1396C suggest multistage events, there is not a clear link between periods of eruptive activity and the occurrence of shelf collapses and initiation of density-currents (Figures 10 and 11). A single density-current deposit within Hole U1396C does, however, appear to be associated with eruptive activity. Unit C preserves a single marine tephra layer interbedded between bioclast-rich volcaniclastic density-current deposits, with no hemipelagic sediment in between. This may suggest that the collapse and resulting density-current occurred in immediate association with the eruption. However, complicated sedimentation processes at Site U1396 also mean that this association may have been artificially produced by winnowing and erosion. Recent activity of the Soufrière Hills volcano has shown that eruptive activity can directly produce density-current deposits [*Trofimovs et al*., 2013]. The eruptive activity at 8–12 ka is closely connected to a powerful density-current, which caused large-scale erosion, demonstrating this association. However, not all eruptions generate widespread fall deposits, and some fallout may be preserved as cryptotephras; therefore, associations between eruptive activity and density-current deposits can be difficult to identify. Only core JC18–19 has been investigated for cryptotephra layers, and hence a number of volcanic events may be present within previously studied cores, but have not been identified. Thus, improvements in the detection of these volcanic events may yet reveal a more robust association between eruptive and density current activity.

To the south east of Montserrat, within the Bouillante-Montserrat Graben, *Trofimovs et al*. [2013] found that the initiation of submarine landslides through volcano flank and carbonate shelf collapses, was not dependent on contemporaneous eruptions. *Trofimovs et al*. [2013] suggested that other factors triggered these events, such as seismic activity, sea level fluctuations and climate-induced sediment loading on submarine shelves. A tentative correlation can be made between more vigorous activity on Montserrat and changes in global (eustatic) sea level and climate (Figure 11). More frequent events are recorded at Site U1396 during transitions between MIS, which indicate changes in sea level (Figure 11). If this association is correct, then it has important implications for hazard prediction. However, the current sedimentary record offshore of Montserrat only extends through two major climate cycles and local tectonic uplift or subsidence may have modified the pattern of sea level recorded in this area. In addition, complicated sedimentary processes mean it is not possible to calculate the exact timing of units B and C, thus their association to MIS transitions is not fully understood. A more rigorous statistical analysis and more precise dating would be needed to establish firm links between clusters of events and eustatic sea level.

5. Conclusions

The high-resolution biostratigraphy, geochemistry, and component analyses of the upper ~250 ka of IODP Site U1396 south west offshore Montserrat, Lesser Antilles has enabled us to draw together data from previous studies, identifying the timing of, and potential associations between, events in this area. This study identifies correlations between proximal and distal sites that reveal the spatial extent of large-scale density-current and eruptive fall deposits, further improving our understanding of this large data set.

Five periods of heightened activity were identified at Site U1396 at <12, $\sim 49.5 \pm 1.1$, 57–105 ($\sim 75 \pm 10$), ~105, and ~130 ka. In contrast to CAR-MON 2, the majority of units within Hole U1396C were interpreted

as density-current deposits (A, B, C1, and C3), and only a single visible eruptive fall deposit was identified (C2, potentially also D). Clast componentry permitted the correlation of most of these deposits laterally across previously studied sites, considerably extending their known range. However, a single, coarse, thick, bioclast-rich deposit (Unit A) positioned just below the seafloor has never been described from offshore of Montserrat. The depositional processes of this unit could not be interpreted here, and it is hoped that future research upon short cores (JC83), recently collected close to Site U1396, may help us to interpret the origin of this distinct unit. This study has revealed that a large-scale erosional event, thought to have occurred at 8–12 ka and previously identified within proximal cores, also reached site U1396 and was powerful enough to erode up to 357 cm of sediment 33 km offshore. This has important implications for future stratigraphy at distal sites and for hazard prediction.

A further important finding of this study is the recognition of disruptive effects from localized bottom water currents at Site U1396 and JC18–19. Bottom water currents generated a reduction in the number of holoplanktic gastropods in areas unaffected by dissolution (and where they are otherwise abundant) and modified the overall grain size distribution to coarser values, compared to other offshore sites. The position and extent of such bottom water currents have important implications for future study sites and should be investigated further.

This study demonstrates that multiple cores, and IODP cores in particular, greatly aid detailed interpretations of the chronostratigraphy in complex environments. Our robust stratigraphy at Site U1396 identified critical data to assess the relationship between eruptive activity and volcanic collapse events, which can be further explored by ongoing research on sites drilled during IODP Expedition 340. Montserrat now provides one of the most detailed field data sets available for reconstructing long-term evolution of a volcanic island, from both offshore and terrestrial deposits. The chronostratigraphy of IODP Site U1396 presented here now forms an important part of this data set.

Acknowledgments

All data from this study are available from the British Oceanographic Data Centre's website. This research used samples and/or data provided by the Integrated Ocean Drilling Program (IODP). We would like to thank the crew and technicians who took part in IODP Expedition 340 and the curators of the Gulf Coast Core Repository, Texas, USA, for providing additional samples of U1396C. We are grateful to James McManus for commenting on and providing additional information about organic carbon and carbonate data. We would also like to acknowledge the help of Dave Spanner and Megan Spencer in carrying out oxygen isotope analysis at NOC. This research was carried out with funding from a NERC research grant (NE/K002724/1) awarded to CWS and DW-P. M.C. and S.F.L.W. thank NERC for financial support via grant NE/K000403/1.

References

Allen, S. R., and A. Freundt (2006), Resedimentation of cold pumiceous ignimbrite into water: Facies transformations simulated in flume experiments, *Sedimentology*, *53*, 717–734, doi:10.1111/j.1365-3091.2006.00790.x.

Allen, S. R., A. Freundt, and K. Kurokawa (2012), Characteristics of submarine pumice-rich density current deposits sourced from turbulent mixing of subaerial pyroclastic flows at the shoreline: Field and experimental assessment, *Bull. Volcanol.*, *74*, 657–675, doi:10.1007/s00445-011-0553-1.

Alloway, S. R., et al. (2007), Towards a climate event stratigraphy for New Zealand over the past 30000 years (NZ-INTIMATE project), *J. Quat. Sci.*, *22*, 9–35, doi:10.1002/jqs.1079.

Cande, S. C., and D. V. Kent (1995), Revised calibration of the geomagnetic polarity timescale for the Late Cretaceous and Cenozoic, *J. Geophys. Res.*, *100*, 6093–6095, doi:10.1029/94JB03098.

Carey, S. (1997), Influence of convective sedimentation on the formation of widespread tephra fall layers in the deep sea, *Geology*, *25*, 839–842, doi:10.1130/0091-7613(1997)025<0839:IOCSOT>2.3.CO;2.

Cassidy, M. (2012), The evolution of volcanism on Montserrat, PhD thesis, Sch. of Ocean and Earth Sci., Univ. of Southampton, Southampton, UK.

Cassidy, M., J. Trofimovs, M. R. Palmer, P. J. Talling, S. F. L. Watt, S. Moreton, and R. N. Taylor (2013), Timing and emplacement dynamics of newly recognised mass flow deposits at ~8–12 ka offshore Soufrière Hills volcano, Montserrat: How submarine stratigraphy can complement subaerial eruption histories, *J. Volcanol. Geotherm. Res.*, *253*, 1–14, doi:10.1016/j.jvolgeores.2012.12.002.

Cassidy, M., J. Trofimovs, S. F. L. Watt, M. R. Palmer, R. N. Taylor, T. M. Gernon, P. J. Talling, and A. Le Friant (2014), Multi-stage collapse events in the South Soufriere Hills, Montserrat as recorded in marine sediment cores, in *The Eruption of Soufrière Hills Volcano, Montserrat From 2000 to 2010, Mem. Geol. Soc. London*, vol. 39, edited by G. Wadge et al., pp. 381–395, Geol. Soc. of London, London.

Chaisson, W. P., and P. N. Pearson (1997), Planktonic foraminifera biostratigraphy at Site 925: Middle Miocene–Pleistocene, *Proc. Integrated Ocean Drill. Program*, *154*, 3–31.

Chiocci, F. L., and G. De Alteriis (2006), The Ischia debris avalanche: First clear submarine evidence in the Mediterranean of a volcanic island prehistorical collapse, *Terra Nova*, *18*, 202–209, doi:10.1111/j.1365-3121.2006.00680.x.

Crutchley, G. J., et al. (2013), Insights into the emplacement dynamics of volcanic landslides from high-resolution 3D seismic data acquired offshore Montserrat, Lesser Antilles, *Mar. Geol.*, *335*,1–15, doi:10.1016/j.margeo.2012.10.004.

Deplus, C., A. Le Friant, G. Boudon, J. C. Komorowski, B. Villemant, C. Harford, J. Ségoufin, and J. L. Cheminée (2001), Submarine evidence for large-scale debris avalanches in the Lesser Antilles Arc, *Earth Planet. Sci. Lett.*, *192*, 145–157, doi:10.1016/S0012-821X(01)00444-7.

Druitt, T. H., and B. P. Kokelaar (Eds.) (2002), *The Eruption of Soufrière Hills Volcano, Montserrat From 1995 to 1999, Mem. Geol. Soc.*, vol. 21, Geol. Soc. of London, London.

Ericson, D. B., and G. Wollin (1956), Micropaleontological and isotopic determinations of Pleistocene climates, *Micropaleontology*, *2*, 257–270.

Expedition 340 Scientists (2012), Lesser Antilles volcanism and landslides: Implications for hazard assessment and long-term magmatic evolution of the arc, Prelim. Rep. Integrated Ocean Drill. Program, *340*, 1–130.

Harford, C. L., M. S. Pringle, R. S. J. Sparks, and S. R. Young (2002), The volcanic evolution of Montserrat using $^{40}Ar/^{39}Ar$ geochronology, in *The Eruption of Soufrière Hills Volcano, Montserrat From 1995 to 1999, Mem. Geol. Soc. London*, vol. 21, edited by T. H. Druitt and B. P. Kokelaar, pp. 93–113, Geol. Soc. of London, London.

Hunt, J. E., R. B. Wynn, D. G. Masson, P. J. Talling, and D. A. H. Teagle (2011), Sedimentological and geochemical evidence for multistage failure of volcanic island landslides: A case study from Icod landslide on north Tenerife, Canary Islands, *Geochem. Geophys. Geosyst.*, *12*, Q12007, doi:10.1029/2011GC003740.

Hunt, J. E., R. B. Wynn, P. J. Talling, and D. G. Masson (2013), Multistage collapse of eight western Canary Island landslides in the last 1.5 Ma: Sedimentological and geochemical evidence from subunits in submarine flow deposits, *Geochem. Geophys. Geosyst.*, *14*, 2159–2181, doi:10.1002/ggge.20138.

Imbrie, J., J. D. Hays, D. G. Martinson, A. McIntyre, A. C. Mix, J. J. Morley, N. G. Pisias, W. L. Prell, and N. J. Shackleton (1984), The orbital theory of Pleistocene climate: Support from a revised chronology of the marine δ^{18}O record, in *Milankovitch and Climate: Part 1*, edited by A. L. Berger et al., pp. 269–305, D. Reidel, Hingham, Mass.

Inman, D. L. (1952), Measures for describing the size distribution of sediments, *J. Sediment. Petrol.*, *22*, 125–145.

Kameo, K., and T. J. Bralower (2000), Neogene calcareous nannofossil biostratigraphy of Sites 998, 999, and 1000, Caribbean Sea. Proc. Ocean Drill. Program, *165*, 3–17, doi:10.2973/odp.proc.sr.165.012.2000.

Lea, D. W., P. A. Martin, D. K. Pak, and H. J. Spero (2002), Reconstructing a 350 ky history of sea level using planktonic Mg/Ca and oxygen isotope records from a Cocos Ridge core, *Quat. Sci. Rev.*, *21*, 283–293, doi:10.1016/S0277-3791(01)00081-6.

Lebas, E., A. Le Friant, G. Boudon, S. F. L. Watt, P. J. Talling, N. Feuillet, C. Deplus, C. Berndt, and M. E. Vardy (2011), Multiple widespread landslides during the long-term evolution of a volcanic island: Insights from high-resolution seismic data, Montserrat, Lesser Antilles, *Geochem. Geophys. Geosyst.*, *12*, Q05006, doi:10.1029/2010GC003451.

Le Friant, A., C. L. Harford, C. Deplus, G. Boudon, R. S. J. Sparks, R. A. Herd, and J. C. Komorowski (2004), Geomorphological evolution of Montserrat (West Indies): Importance of flank collapse and 734 erosional processes, *J. Geol. Soc. London*, *161*, 147–160, doi:10.1144/0016-764903-017.

Le Friant, A., E. J. Lock, M. B. Hart, G. Boudon, R. S. J. Sparks, M. J. Leng, C. W. Smart, J. C. Komorowski, C. Deplus, and J. K. Fisher (2008), Late Pleistocene tephrochronology of marine sediments adjacent to Montserrat, Lesser Antilles volcanic arc, *J. Geol. Soc. London*, *165*, 279–290, doi:10.1144/0016-76492007-019.

Le Friant, A., C. Deplus, G. Boudon, N. Feuillet, J. Trofimovs, J.-C. Komorowski, R. S. J. Sparks, P. J. Talling, S. Loughlin, and G. Ryan (2010), Eruption of Soufrière Hills (1995–2009) from an offshore perspective: Insights from repeated swath bathymetry surveys, *Geophys. Res. Lett.*, *37*, L11307, doi:10.1029/2010GL043580.

Le Friant, A., O. Ishizuka, N. A. Stroncik, and Expedition 340 Scientists (2013), *Lesser Antilles Volcanism and Landslides: Implications for Hazard Assessment and Long-Term Magmatic Evolution of the Arc, Proc*. Integrated Ocean Drill. Program, 340, doi:10.2204/iodp.pr.340.2013.

Lowe, D. J. (2011), Tephrochronology and its application: A review, *Mar. Geol.*, *6*, 107–153, doi:10.1016/j.quageo.2010.08.003.

Lowe, D. J., and J. B. Hunt (2001), A summary of terminology used in tephra-related studies, in *Tephras: Chronology, Archaeology*, vol. 1, edited by E. T. Juvigné and J.-P. Raynal, pp. 17–22, CDERAD éditeur, Goudet, France.

Manville, V., and C. J. N. Wilson (2004), Vertical density currents: A review of their potential role in the deposition and interpretation of deep-sea ash layers, *J. Geol. Soc. London*, *161*, 947–958, doi:10.1144/0016-764903-067.

Martinson, D. G., N. G. Pisias, J. D. Hays, J. Imbrie, T. C. Moore Jr., and N. J. Shackleton (1987), Age dating and the orbital theory of the ice ages: Development of a high-resolution 0 to 300,000-year chronostratigraphy, *Quat. Res.*, *27*, 1–29, doi:10.1016/0033-5894(87)90046-9.

Masson, D. G., C. B. Harbitz, R. B. Wynn, G. Pedersen, and F. Lovholt (2006), Submarine landslides: Processes, triggers and hazard prediction, *Philos. Trans. R. Soc. A*, *364*, 2009–2039, doi:10.1098/rsta.2006.1810.

Moore, J. G., W. R. Normark, and R. T. Holcomb (1994), Giant hawaiian landslides, *Annu. Rev. Earth Planet. Sci.*, *22*, 119–144, doi:10.1146/annurev.ea.22.050194.001003.

Paulatto, M., C. Annen, T. J. Henstock, E. Kiddle, T. A. Minshull, R. S. J. Sparks, and B. Voight (2012), Magma chamber properties from integrated seismic tomography and thermal modelling, Montserrat, *Geochem. Geophys. Geosyst.*, *13*, Q01014, doi:10.1029/2011GC003892.

Prell, W. L., J. Imbrie, D. G. Martinson, J. J. Morley, N. G. Pisias, N. J. Shackleton, and H. F. Streeter (1986), Graphic correlation of oxygen isotope stratigraphy application to the late Quaternary, *Paleoceanography*, *1*, 137–162, doi:10.1029/PA001i002p00137.

Reid, R. P., S. N. Carey, and D. R. Ross (1996), Late Quaternary sedimentation in the Lesser Antilles island arc, *Geol. Soc. Am. Bull.*, *108*, 78–100, doi:10.1130/0016-7606(1996)108<0078:LQSITL>2.3.CO;2.

Schindlbeck, J. C., S. Kutterolf, A. Freundt, R. P. Scudder, K. T. Pickering, and R. W. Murray (2013), Emplacement processes of submarine volcaniclastic deposits (IODP Site C0011, Nankai Trough), *Mar. Geol.*, *343*, 115–124, doi:10.1016/j.margeo.2013.06.017.

Silver, E., et al. (2005), Island arc debris avalanches and tsunami generation, *Eos Trans. AGU*, *86*, 485–489, doi:10.1029/2005EO470001.

Smith, A. L. R., M. J. Schellekens, J. H. Schellekens, and G. S. Mattioli (2007), Prehistoric stratigraphy of the Soufrière Hills–South Soufrière Hills volcanic complex, Montserrat, West Indies, *J. Geol.*, *115*, 115–127, doi:10.1086/509271.

Sparks, R. S. J., J. Barclay, E. S. Calder, R. A. Herd, J. C. Komorowski, R. Luckett, G. E. Norton, L. J. Ritchie, B. Voight, and A. W. Woods (2002), Generation of a debris avalanche and violent pyroclastic density current on 26 December (Boxing Day) 1997 at Soufriere Hills Volcano, Montserrat, *The eruption of Soufrière Hills Volcano, Montserrat, from 1995 to 1999, Mem. Geol. Soc. London*, vol. 21, edited by T. H. Druitt and B. P. Kokelaar, pp. 409–434, Geol. Soc. of London, London, U. K.

Trofimovs, J., et al. (2006), Submarine pyroclastic deposits formed at the Soufrière Hills Volcano, Montserrat (1995–2003): What happens when pyroclastic flows enter the ocean?, *Geology*, *34*, 549–552, doi:10.1130/G22424.1.

Trofimovs, J., et al. (2010), Evidence for carbonate platform failure during rapid sea-level rise; *ca* 14000 year old bioclastic flow deposits in the Lesser Antilles, *Sedimentology*, *57*, 735–759, doi:10.1111/j.1365-3091.2009.01117.

Trofimovs, J., et al. (2012), Submarine pyroclastic deposits formed during the 20th May 2006 dome collapse of the Soufrière Hills Volcano, Montserrat, *Bull. Volcanol.*, *74*, 391–405, doi:10.1007/s00445-011-0533-5.

Trofimovs, J., et al. (2013), Timing, origin and emplacement dynamics of mass flows offshore of SE Montserrat in the last 110 ka: Implications for landslide and tsunami hazards, eruption history and volcanic island evolution, *Geochem. Geophys. Geosyst.*, *14*, 385–406, doi:10.1002/ggge.20052.

Wade, B. S., P. N. Pearson, W. A. Berggren, and H. Pälike (2011), Review and revision of Cenozoic tropical planktonic foraminiferal biostratigraphy and calibration to the geomagnetic polarity and astronomical time scale, *Earth Sci. Rev.*, *104*, 111–142, doi:10.1016/j.earscirev.2010.09.003.

Wadge, G., et al. (Eds.) (2014), *The Eruption of Soufrière Hills Volcano, Montserrat From 2000 to 2010, Mem. Geol. Soc. London*, vol. 39, Geol. Soc. of London, London, U. K.

Wall-Palmer, D. (2013), The response of pteropod and related faunas to climate change and ocean acidification, PhD thesis, Sch. of Geogr., Earth and Environ. Sci., Plymouth Univ., Plymouth, U. K.

Wall-Palmer, D., C. W. Smart, and M. B. Hart (2013), In-life pteropod dissolution as an indicator of past ocean carbonate saturation, *Quat. Sci. Rev.*, *81*, 29–34, doi:10.1016/j.quascirev.2013.09.019.

Watt, S. F. L., et al. (2012a), Combinations of volcanic-flank and seafloor-sediment failure offshore Montserrat and their implications for tsunami generation, *Earth Planet. Sci. Lett.*, *319–320*, 228–240, doi:10.1016/j.epsl.2011.11.032.

Watt, S. F. L., et al. (2012b), Widespread and progressive seafloor-sediment failure following volcanic debris avalanche emplacement: Landslide dynamics and timing offshore Montserrat, Lesser Antilles, *Mar. Geol.*, *323–325*, 69–94, doi:10.1016/j.margeo.2012.08.002.

Waythomas, C. F., P. Watts, F. Shi, and J. T. Kirby (2009), Pacific Basin tsunami hazards associated with mass flows in the Aleutian arc of Alaska, *Quat. Sci. Rev.*, *28*, 1006–1019, doi:10.1016/j.quascirev.2009.02.019.

Ziebis, W., J. McManus, T. Ferdelman, F. Schmidt-Schierhorn, W. Bach, J. Muratli, K. J. Edwards, and H. Villinger (2012), Interstitial fluid chemistry of sediments underlying the North Atlantic gyre and the influence of subsurface fluid flow, *Earth Planet. Sci. Lett.*, *323–324*, 79–91, doi:10.1016/j.epsl.2012.01.018.